AGU100 ADVANCING EARTH AND SPACE SCIENCE

JGR Planets

Key Points:
- First multiyear in situ measurements of the major components of the Mars atmosphere have been obtained by the MSL/SAM investigation
- Seasonal variation of CO_2, N_2, and Ar reveals differences in atmospheric transport and mixing timescales
- Oxygen varies seasonally and interannually, independently from Ar and N_2, on timescales too fast to be explained by known chemistry

Supporting Information:
- Supporting Information S1
- Table S1
- Table S2

Correspondence to:
M. G. Trainer,
melissa.trainer@nasa.gov

Seasonal Variations in Atmospheric Composition as Measured in Gale Crater, Mars

Melissa G. Trainer[1] (iD), **Michael H. Wong**[2] (iD), **Timothy H. McConnochie**[3], **Heather B. Franz**[1], **Sushil K. Atreya**[2], **Pamela G. Conrad**[4], **Franck Lefèvre**[5], **Paul R. Mahaffy**[1] (iD), **Charles A. Malespin**[1], **Heidi L.K. Manning**[6], **Javier Martín-Torres**[7,8], **Germán M. Martínez**[9,2], **Christopher P. McKay**[10], **Rafael Navarro-González**[11] (iD), **Álvaro Vicente-Retortillo**[2], **Christopher R. Webster**[12], and **María-Paz Zorzano**[13,7] (iD)

[1]NASA Goddard Space Flight Center, Greenbelt, MD, USA, [2]Climate and Space Sciences and Engineering, University of Michigan, Ann Arbor, MI, USA, [3]University of Maryland, College Park, MD, USA, [4]Geophysical Laboratory, Carnegie Institution of Washington, Washington, DC, USA, [5]LATMOS, CNRS, Sorbonne Université, UVSQ, Paris, France, [6]College of Arts and Sciences, Misericordia University, Dallas, PA, USA, [7]Department of Computer Science, Electrical and Space Engineering, Luleå University of Technology, Luleå, Sweden, [8]Instituto Andaluz de Ciencias de la Tierra (CSIC-UGR), Granada, Spain, [9]Lunar and Planetary Institute, Universities Space Research Association, Houston, TX, USA, [10]NASA Ames Research Center, Moffett Field, CA, USA, [11]Instituto de Ciencias Nucleares, Universidad Nacional Autónoma de México, Ciudad de México, Mexico, [12]NASA Jet Propulsion Laboratory, California Institute of Technology, Pasadena, CA, USA, [13]Centro de Astrobiología (INTA-CSIC), Torrejón de Ardoz, Madrid, Spain

Abstract The Sample Analysis at Mars (SAM) instrument onboard the Mars Science Laboratory Curiosity rover measures the chemical composition of major atmospheric species (CO_2, N_2, ^{40}Ar, O_2, and CO) through a dedicated atmospheric inlet. We report here measurements of volume mixing ratios in Gale Crater using the SAM quadrupole mass spectrometer, obtained over a period of nearly 5 years (3 Mars years) from landing. The observation period spans the northern summer of MY 31 and solar longitude (L_S) of 175° through spring of MY 34, $L_S = 12°$. This work expands upon prior reports of the mixing ratios measured by SAM QMS in the first 105 sols of the mission. The SAM QMS atmospheric measurements were taken periodically, with a cumulative coverage of four or five experiments per season on Mars. Major observations include the seasonal cycle of CO_2, N_2, and Ar, which lags approximately 20–40° of L_S behind the pressure cycle driven by CO_2 condensation and sublimation from the winter poles. This seasonal cycle indicates that transport occurs on faster timescales than mixing. The mixing ratio of O_2 shows significant seasonal and interannual variability, suggesting an unknown atmospheric or surface process at work. The O_2 measurements are compared to several parameters, including dust optical depth and trace CH_4 measurements by Curiosity. We derive annual mean volume mixing ratios for the atmosphere in Gale Crater: $CO_2 = 0.951$ (± 0.003), $N_2 = 0.0259$ (± 0.0006), $^{40}Ar = 0.0194$ (± 0.0004), $O_2 = 1.61$ (± 0.09) x 10^{-3}, and CO = 5.8 (± 0.8) x 10^{-4}.

Plain Language Summary The atmosphere of Mars is made up of primarily carbon dioxide, and during the Martian year, the barometric pressure is known to cycle up and down substantially as this carbon dioxide freezes out and then is rereleased from polar caps. The Mars Science Laboratory Curiosity rover has now acquired atmospheric composition measurements at the ground over multiple years, capturing the variations in the major gases over several seasonal cycles for the first time. With the Sample Analysis at Mars instrument, the annual average composition in Gale Crater was measured as 95.1% carbon dioxide, 2.59% nitrogen, 1.94% argon, 0.161% oxygen, and 0.058% carbon monoxide. However, the abundances of some of these gases were observed to vary up to 40% throughout the year due to the seasonal cycle. Nitrogen and argon follow the pressure changes but with a delay, indicating that transport of the atmosphere from pole to pole occurs on faster timescales than mixing of the components. Oxygen has been observed to show significant seasonal and year-to-year variability, suggesting an unknown atmospheric or surface process at work. These data can be used to better understand how the surface and atmosphere interact as we search for signs of habitability.

1. Introduction

The present-day 25.2° axial tilt or obliquity of Mars is similar to the Earth's 23.5°, resulting in seasonal changes as on Earth. However, each season on Mars is nearly twice as long as on Earth due to Mars'

longer orbital period of 687 days compared to the Earth's 365 days, and the more elliptical orbit of Mars strongly affects the seasonal variation as compared to Earth. The seasonal change in Mars' meteorological parameters has been monitored by a number of spacecraft, beginning with the Viking landers (VL1 and VL2) in 1976 and continuing to this day on the Curiosity rover. As a result, a long time record of the surface pressure and temperature has become available, largely from VL1 and VL2 from MY 12 to MY 15 at their respective landing sites of 22.4°N and 47.9°N, MER-A (Spirit) and MER-B (Opportunity) from MY 26 to MY 33 at 14.6°S and 1.9°S, and now Curiosity at Gale Crater from MY 31 to present at 4.6°S. Other environmental properties, including aerosol opacity, UV flux, relative humidity, and water vapor content, are also being measured on the Curiosity rover (Martínez et al., 2017). These parameters are valuable for interpreting the observations of seasonal, temporal, or sporadic changes in other atmospheric properties such as the abundances of atmospheric volatiles, which are the focus of this paper.

Prior to Curiosity, little information was available on long-term trends in the behavior of the atmospheric constituents. While the GCMS on the Viking landers measured the bulk volume mixing ratios (VMR) of the main atmospheric constituents CO_2, N_2, and ^{40}Ar (95.3%, 2.7%, and 1.6%, respectively), O_2 and CO had large uncertainties (Owen, 1992; Owen et al., 1977; Oyama & Berdahl, 1977). No useful information about their temporal or seasonal change could be derived from those data; however, on the other hand, the seasonal change in surface pressure measured by Viking was instrumental in understanding the unique annual cycle of condensation and sublimation of atmospheric carbon dioxide to and from the poles of Mars (Hess et al., 1980; James et al., 1992). As CO_2 is the principal component of the atmosphere, and the other two gases N_2 and Ar are not condensable at Martian temperatures and pressures, the observed change in the surface pressure can be attributed to seasonal change in the atmospheric CO_2 content. Those data also revealed a time lag between the onset of CO_2 deposition/sublimation and the resulting surface pressure change, which is related to the dynamics of CO_2 migration to and from the poles.

Seasonal variation of the second most abundant gas on Mars, N_2, could not be studied in situ or by remote sensing before Curiosity. However, the next most abundant constituent, radiogenic argon (^{40}Ar, referred to generally as Ar), was measured over several years in situ by the APXS instrument on MER (VanBommel et al., 2018) and by remote sensing using the gamma subsystem of the gamma ray spectrometer on Mars Odyssey orbiter (Sprague et al., 2012). The MER data correspond to the equatorial region, where the VMR of Ar were found to have a relatively small seasonal variation of 10%. The Mars Odyssey data lacked the precision for such small changes in Ar in the equatorial region but revealed a dramatic change in Ar over the poles. The Ar mixing ratio was found to increase by a factor of 6 over the southern pole in winter and by a factor of 3 over the northern pole in winter. As argon is a noncondensable gas, its total atmospheric content remains unchanged through the Martian seasons. The observed seasonal variation in its mixing ratio is therefore due to the dynamical processes induced by the deposition and sublimation of the principal atmospheric constituent, CO_2, at the poles.

Like N_2 and Ar, O_2 and CO are long-lived constituents on Mars, with lifetimes greater than the year on Mars (Atreya & Gu, 1995; Krasnopolsky, 1993; Wong et al., 2003). Besides aforementioned Viking measurements, only a few sporadic ground-based measurements of O_2 were available pre-Curiosity. However, an extensive set of data on CO has been collected between MY 28 and MY 33 by CRISM on MRO (Smith et al., 2017). The CO VMRs from those orbital observations are found to be generally slightly larger than the values obtained from the Earth or from Mars Express observations for corresponding regions (e.g., Billebaud et al., 2009; Encrenaz et al., 2006; Krasnopolsky, 2015).

The SAM results discussed in this paper provide the first simultaneous measurements in the equatorial region of all key constituents. Including CO_2, N_2, Ar, O_2, and CO, these measurements were made over nearly 6 years using the same mass spectrometer of the SAM instrument suite. Additionally, methane has been measured over the same period with the tunable laser spectrometer (TLS) of the SAM suite. Mars is found to have a persistent low background level of methane (CH_4) with a mean value of 0.41 ± 0.16 ppbv, but it undergoes an unexpected seasonal variation of a factor of ~3 from 0.24 to 0.65 ppbv. The observed variation is unrelated to any known environmental factors, which can account for only about ±20% seasonal change in CH_4. The magnitude of the seasonal change in the CH_4 background is much greater than in other long-lived atmospheric volatiles (N_2, Ar, O_2, and CO) discussed in this paper. The TLS results on the methane background and occasional spikes have been published elsewhere (Webster et al., 2015; Webster et al., 2018).
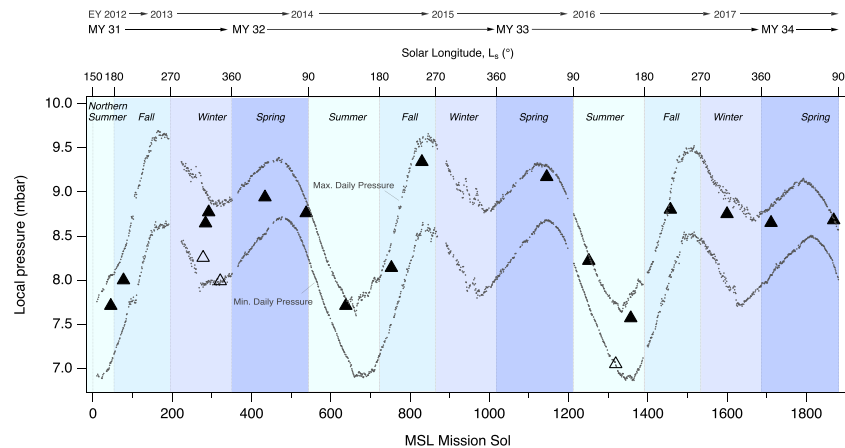
Figure 1. The timing of SAM atmospheric QMS experiments is plotted as the atmospheric pressure at the time of ingestion (left axis) against the MSL mission sol (bottom axis) and solar longitude (top axis). The majority of the atmospheric ingests for mixing ratio derivation was conducted during local night (closed symbols), with three daytime experiments (open symbols). The figure background is shaded by northern season, and the REMS daily pressure maximum and minimum values are given by the dotted lines. Seasonal trends are tracked through the direct atmospheric runs, with attention paid to possible diurnal variations. Mars year (MY) and Earth year (EY) are indicated across the top of the figure.

2. Methods

2.1. SAM QMS Measurements

We report here the measurements of atmospheric volume mixing ratios on Mars using the SAM QMS onboard the Mars Science Laboratory Curiosity rover, taken in Gale Crater (4.5°S, 137°E) over a period of almost 3 Mars years (>5 Earth years) from landing (Vasavada et al., 2014). Although Gale Crater is located just south of the equator, in this paper, the seasons will be referenced with respect to the northern hemisphere. The observation period spans the northern summer of MY 31, solar longitude (L_S) of 175°, and through northern spring of MY 34, $L_S = 85°$. During the measurement timeframe, Curiosity traversed a distance of over 16 km in Gale Crater, spanning elevations from –20 to +329 m relative to the landing site (–4501 m). The SAM QMS atmospheric measurements were taken periodically during this time, interspersed between solid sample measurements and other rover activities, with a cumulative coverage of four or five experiments per season (Figure 1).

Atmospheric mixing ratios measured by the SAM QMS were reported for the first 105 sols of the mission (Mahaffy et al., 2013). These were recently updated to account for newly developed calibration factors following in situ calibration experiments using SAM's onboard calibration cell (Franz et al., 2017). Periodic sampling has continued throughout the mission to explore variations related to the seasonal CO_2 cycle, as indicated by the annual pressure curves (Figure 1). The SAM atmospheric measurements taken through MY 34 L_S 85° overlap seasonally with the first reported measurements in MY 31, testing whether there is a repeatable annual cycle in the atmospheric composition. With the exception of three daytime runs, atmospheric ingestions were taken near local midnight (Table 1).

Following the acquisition of the atmospheric data set presented in this manuscript, the SAM instrument completed its first full derivatization experiment on the Ogunquit Beach (OG) dune sample (Malespin et al., 2018). High signal levels in the wet chemistry experiment on sol 1909 (December, 2017) caused a shift in the sensitivity of the instrument detectors, requiring a change in the QMS electron multiplier gain setting. The gain state change restored QMS count rates to their previous levels, but detailed analysis is ongoing to ensure that deadtime corrections and calibration constants for all species are adjusted. Thus, this report is restricted in scope to atmospheric measurements prior to sol 1909.

2.1.1. Experimental Details and Calibration

The SAM instrument suite consists of three instruments supported by a gas separation and processing subsystem and a solid sample manipulation system (Mahaffy et al., 2012). Results presented here were obtained with the QMS through a dedicated heated (50 °C) atmospheric inlet. The QMS employs
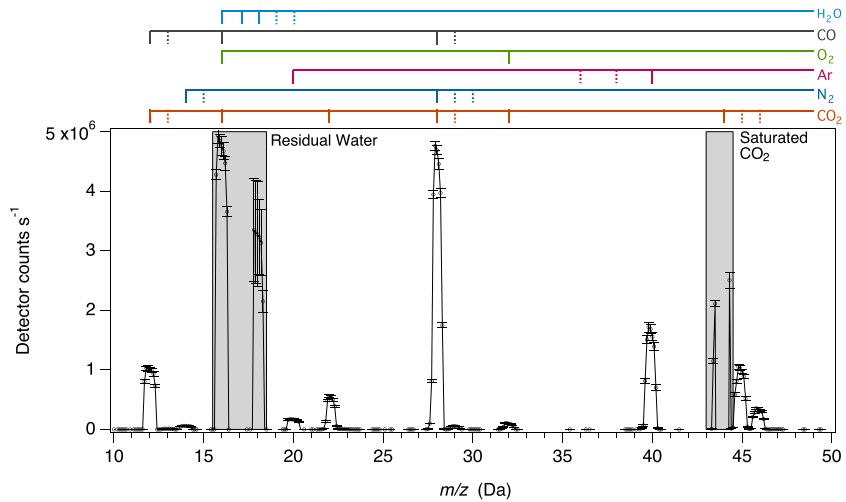
Table 1

SAM Atmospheric Ingest Conditions with Test Identification Numbers (TIDs).

Mars year	Test ID (TID)	MSL sol	L_s (°)	Ingest start LMST	REMS air temp (°C)		REMS ground temp (°C)		REMS pressure (mbar)	
31	25012	45.95	175.59	22:43	−59	±3	−71	±2	7.71	±0.07
	25027	77.88	194.34	21:07	−54	±1	−65	±2	7.94	±0.03
		77.95	194.38	22:42	−57	±1	−69	±3	8.06	±0.03
	25084[a]	278.54	320.77	13:02	−22	±1	−8	±2	8.36	±0.04
		278.61	320.81	14:36	−16	±2	−7	±1	8.15	±0.04
	25088	284.96	324.48	22:55	−49	±1	−58	±2	8.61	±0.04
		285.02	324.51	00:30	−58	±1	−62	±2	8.68	±0.04
	25095	292.10	328.56	2:25	−64	±1	−66	±2	8.75	±0.04
		292.17	328.60	4:00	−66	±1	−69	±2	8.79	±0.04
	25106[a]	321.67	344.92	16:06	−18	±0	−8	±1	8.02	±0.05
		321.74	344.95	17:41	−24	±0	−24	±1	7.96	±0.05
32	25150	434.88	40.89	21:07	−65	±1	−67	±2	8.90	±0.04
		434.95	40.92	22:41	−70	±7	−71	±3	8.97	±0.06
	25172	538.94	87.87	22:30	−74	±7	−74	±5	8.70	±0.06
		539.00	87.90	0:05	−74	±1	−75	±3	8.81	±0.04
	25195	638.05	134.67	1:05	−73	±1	−75	±3	7.70	±0.04
		638.11	134.70	2:39	−78	±1	−80	±3	7.71	±0.04
	25217	753.93	198.85	22:24	−57	±4	−65	±3	8.12	±0.06
		754.00	198.89	23:58	−62	±1	−67	±2	8.15	±0.04
	25232	830.88	247.83	21:05	−47	±1	−53	±2	9.27	±0.04
		830.94	247.87	22:40	−51	±1	−57	±3	9.40	±0.04
33	25301	1145.96	60.21	22:57	−68	±3	−71	±3	9.09	±0.04
		1146.02	60.24	0:32	−68	±1	−75	±3	9.24	±0.04
	25337	1251.98	108.28	23:37	−75	±1	−79	±3	8.19	±0.05
		1252.05	108.32	1:12	−79	±1	−81	±3	8.25	±0.05
	25343[a]	1319.68	141.28	16:18	−26	±1	−25	±2	7.05	±0.05
	25346	1357.07	161.02	01:46	−69	±5	−72	±3	7.57	±0.05
	25372	1457.07	220.39	01:35	−60	±1	−64	±2	8.80	±0.05
	25395	1600.07	311.55	01:46	−62	±1	−69	±3	8.75	±0.05
34	25409	1711.06	11.86	01:26	−67	±1	−73	±2	8.65	±0.05
	25440	1869.07	84.70	01:42	−73	±2	−82	±5	8.68	±0.07

[a]Daytime ingest.

hyperbolic rods, redundant 70-eV electron beam energy ion sources, and redundant pulse counting Channeltron detectors. Separate miniaturized turbomolecular pumps (compression ratio ~5×10^8) evacuate the small QMS sensor volume and the much larger inlet manifold volume prior to Martian atmosphere ingestion. Experiments include two background scans: One with the QMS sensor volume isolated from the manifold and one with the QMS open to the evacuated manifold. The QMS is operated in a dynamic sampling mode with continuous pumping by one of the turbomolecular pumps. An atmospheric sample is acquired by opening a valve on the sample inlet tube for ~30 sec to introduce gas to a portion of the manifold. A small fraction of this gas is then leaked into the QMS and scanned over a specified mass range (1.5–149.9 Da) for several minutes. This process is repeated for most runs to provide two ingestions per experiment (Table 1). Detailed descriptions of the experimental design and flight instrument calibration for the atmospheric investigation can be found in Franz et al. (2014).

Direct atmospheric QMS data were acquired in both a fractional scan mode with 0.1-Da step size and a unit scan mode with 1.0-Da step size. A typical fractional scan spectrum acquired during an atmospheric experiment is shown in Figure 2. Fractional scan mode reduces uncertainties related to the tuning and shape of spectral peaks, while unit scan mode reduces uncertainties due to time variation in the signal (as both background and sample are pumped out). Repeated experiments have shown that sample and background signals are well characterized by exponential functions of time, so best results are determined through processing of data acquired in fractional scan mode (Franz et al., 2014; Franz et al., 2015). The method involves correcting mass spectra for detecting deadtime effects at high count rates and integrating peak areas (±0.4 Da) for the m/z values of the major atmospheric components, CO_2, Ar, N_2, O_2, and CO.

Figure 2. A typical atmospheric mass spectrum taken in fractional scan mode with the residual background signal subtracted. TID 25217 is shown here; see Table 1 for details. The error bars show the standard deviation of the average counts per second (cps) from multiple scans over a ~7-minute period. The gray bars indicate regions of the spectrum which are not used for VMR calculations, either due to decreasing residual water signal or high counts from the primary CO_2 ion (m/z 44) that saturate the detector. Integrated peak areas used for quantitative determination of the volume mixing ratios are determined from a +/-0.4 Da window around each nominal m/z.

Data corrections are needed to account for isobaric interference (multiple species contributing to count rates at a single m/z value) and for pressure-related variation in CO_2-splitting fractions (ratios between yields of products such as CO_2^+, CO_2^{++}, and O_2^+ upon ionization of atmospheric CO_2 molecules). As described in Franz et al. (2015), calibration experiments on the SAM flight instrument and laboratory QMS test bed have demonstrated an increase with pressure in the ratio of doubly to singly ionized CO_2. The high abundance of CO_2 in atmospheric samples leads to saturation at m/z 44 (Figure 2), so we rely on the CO_2^{++} signal at m/z 22 as the reference marker for mixing ratio measurements. We adjust for the pressure dependence of the CO_2^{++}-/CO_2^+-splitting fraction using empirical corrections from Franz et al. (2015):

$$m22_{corr} = F_{22} \times m22_{obs}, \tag{1}$$

where the correction factor is a linear function of the uncorrected count ratio at m/z 22:

$$F_{22} = a \times m22_{obs} + b, \tag{2}$$

with coefficients $a = -2.321$ (± 0.1094) x 10^{-7} cps^{-1} and $b = 1.000 \pm 0.003$. To isolate the signal at m/z 32 due to atmospheric O_2 ($m32_{corr}$) from the observed signal at m/z 32 ($m32_{obs}$), we apply an assumption that the O_2^+/CO_2^+ splitting fraction is pressure invariant. For the atmospheric data in which the $m44$ peak is saturated, the correction is applied as follows:

$$m32_{corr} = m32_{obs} - c \times (m44/m22)_{CO2} \times m22_{corr}, \tag{3}$$

where $c = 4.558$ (± 0.07104) x 10^{-4} and $(m44/m22)_{CO2} = 145.88 \pm 1.17$ as in Tables 1 and 2, respectively, in Franz et al. (2015).

Overall sources of error in the mixing ratio calculation include (i) measurement noise (detector noise following Poisson counting statistics), (ii) errors in the data corrections (detector deadtime, background subtractions, and isobaric interferences), and (iii) uncertainties in the calibration constants. Some of these errors can be reduced by averaging data points within individual experiments and by averaging multiple experiments (i.e., measurement noise and background subtractions), while other sources are systematic and are not reduced by averaging multiple experiments together (i.e., calibration constants and corrections for deadtime and isobaric interference). Discussions of these sources of error and their estimation are included in Franz et al. (2014) and in the supplemental material of Wong, Atreya, et al. (2013). For the
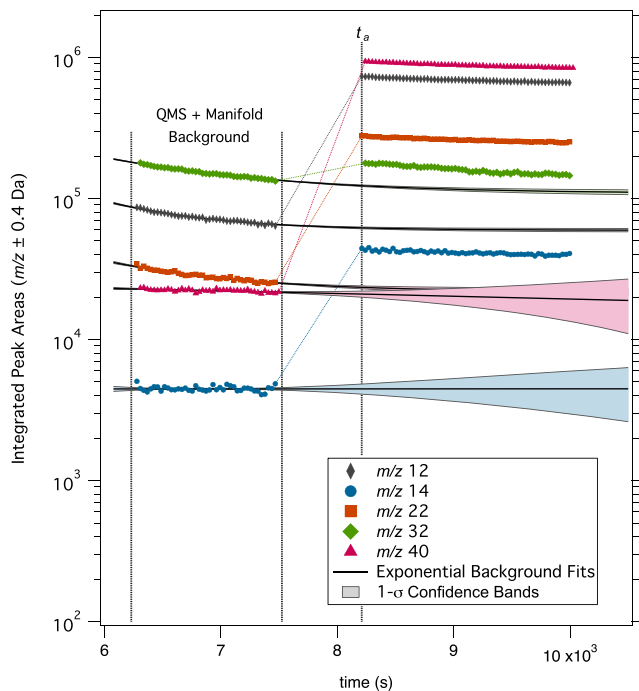
Figure 3. Integrated peak areas (cps * 0.8 Da-width peak) for the preferred ions of CO_2 (m/z 22), Ar (m/z 40), N_2 (m/z 14), O_2 (m/z 32), and CO (m/z 12, with contributions from CO_2) are plotted against time for a typical SAM atmospheric experiment. TID 25217 is shown here; see Table 1 for details. The background measurement (no atmospheric gas ingested into the QMS) is accomplished in the experiment time between 6,278 and 7,468 s. Mars atmosphere is then ingested and measured by the mass spectrometer between 8,211 and 10,000 s. To perform the background correction, the exponential decay in the residual gas background signal shown in the bracketed region is fit and extrapolated to the time of the first fractional atmospheric scan at time t_a. The fit value at t_a is then used to estimate the contribution of the background to the signal during the sample ingest. As can be seen in this example, only the m/z 32 background is >10% of the atmospheric signal. Confidence bands show the fit uncertainties used to estimate the error in the background correction.

major atmospheric gases with multiple ion fragments measured by the QMS, the m/z values used for calculation of mixing ratios were selected to have large enough count rates to minimize detector noise but low enough count rates to minimize saturation and deadtime effects. Although contributions of residual gas molecules to the background are minimal for most species, the background signal for the primary peak for O_2 (m/z 32) is high, thus a large proportion of the total signal. This is due to O_2 permeation from the high conductance valve seat after opening, and the background signal decreases exponentially once the QMS and manifold are actively evacuated. This background correction is therefore challenging and is a major source of uncertainty in the O_2 mixing ratios measured by the SAM QMS (see Figure S3 of the supporting information).

Figure 3 shows a typical experiment timeline with backgrounds and atmospheric samples for the primary atmospheric species of interest. The approach used for the background correction is to fit an exponential signal as a function of time to the data within the background interval (specifically, the background scan with the QMS exposed to the evacuated manifold) and extrapolating to the sample interval to determine the time-dependent background signal. This correction is a small percentage of the total signal for four of the species under study and thus introduces a minor uncertainty to the final mixing ratio. For the O_2 peak at m/z 32, the correction is a large proportion of the signal ($\geq 50\%$) and varies between different experiments and different ingested samples within each experiment. To accurately capture the inherent uncertainty in this correction in the O_2 mixing ratio, the 1-σ confidence intervals for the exponential fit at t_a are included as part of the error estimation. Our uncertainty estimates include variations in the functional form of the background fit, in specific cases where the form of the fit significantly influenced the results.

As seen in Figure 3, the magnitude of the QMS signal for the atmospheric sample is also a time variable, as the sample trapped in the manifold is gradually pumped through the QMS. Ratios for the major ions of each gas are taken at each time point (i.e., from each mass spectrum) and then averaged to remove the time variability from the mixing ratio determinations. Resulting ratios are constant across a sampling interval. Mixing ratios are then computed at each time point and averaged for each ingestion. For experiments with two atmospheric ingests, the resulting mixing ratios from each ingestion are combined into a weighted mean for the sol, reducing systematic errors due to the background corrections. The values reported in Table S1 are these weighted means.

Finally, for CO_2, the calculated uncertainties in the reported mixing ratios in this manuscript differ from those in the previous publications (Franz et al., 2014; Franz et al., 2015; Franz et al., 2017; Mahaffy et al., 2013). For this work, we are most interested in identifying seasonal trends and therefore relative behavior of the measured mixing ratios throughout the mission. For CO_2 in particular, the errors previously reported are largely introduced by the uncertainty in the calibration constant derived during the prelaunch calibration. This constant introduces an uncertainty on the CO_2 VMR on the order of 3%. This uncertainty would apply to the absolute amount of CO_2 (such as a calculated partial pressure or number density) but is not optimal for characterizing the VMR. The uncertainty on the relative abundance of CO_2 is best modeled by assuming that the total atmospheric composition must be equal to 1 and thus the uncertainty on the CO_2 is equal to the total uncertainties on the trace gases (Ar, N_2, O_2, and CO, added in quadrature) that comprise the balance of the atmosphere.

2.2. Supporting Curiosity Measurements
2.2.1. Rover Environmental Monitoring Station
Throughout the mission, meteorological conditions along the traverse in Gale Crater have been measured by the Rover Environmental Monitoring Station (REMS) sensor suite (Gómez-Elvira et al., 2012). The REMS
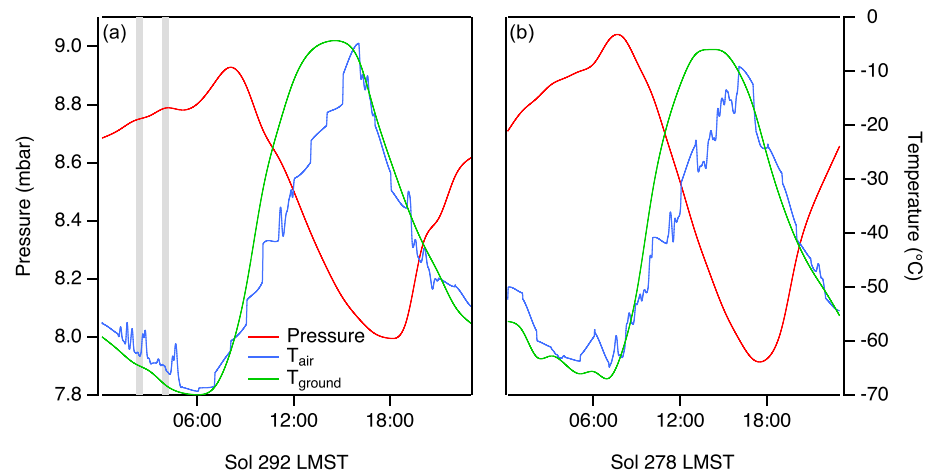
Figure 4. The QMS sample ingestion times are shown in the context of the daily pressure and temperature cycles for **(a)** a typical nighttime ingestion, sol 292, and **(b)** one of the daytime ingestions, sol 278. The temperature at the SAM QMS inlet (at approximately 1 m) is between the values measured for the ground (0 m) and by the atmospheric sensor on the rover mast (1.6 m).

suite performs measurements of atmospheric pressure, ground and atmospheric temperatures, atmospheric relative humidity, UV radiation fluxes, and horizontal wind speeds (e.g., Martínez et al., 2017). To provide context for the SAM VMR measurements and the seasonal behavior of the major gases, we focus primarily on the analysis of REMS pressure (P) and atmospheric temperature (T) measurements. Comparisons to other environmental conditions, including those measured by REMS, are discussed below in section 4.2, with more detail in the supporting information Figure S7.

The pressure and temperature conditions at the time of sample ingestion for each QMS experiment are provided in Table 1. Conditions were calculated as described in Wong, LeFavor, et al. (2013). Uncertainties include estimated extrapolation uncertainties at times when simultaneous REMS measurements are not available, variation over the duration of the ingest event, and instrumental uncertainties. Updated instrumental uncertainty values correspond to the 9th PDS data release. Ingest start times are rounded to the nearest minute, in local mean solar time (LMST). As indicated in the table, the majority of the atmospheric samples was acquired in near midnight. Three experiments were conducted in the midafternoon to late afternoon, two of these in close proximity to nighttime experiments (within ten sols). Figure 4 shows the daily temperature and pressure curves for two of the sols in which the QMS sampled, 292 and 278, acquired during northern winter/southern summer. The vertical gray bars indicate the times of the QMS sample ingestions, showing a typical nighttime experiment and one of the daytime experiment. The search for possible diurnal trends was of interest in part because of the large diurnal pressure variations observed in Gale Crater, driven by a combination of thermal tides and topographical effects. Haberle et al. (2014) discussed this in their interpretation of the pressure cycles over the first 100 sols on Mars, concluding that in addition to the global thermal tides in the atmosphere from solar heating, the diurnal cycle of upslope/downslope flows driving crater circulation likely have a significant effect on the pressure amplitudes, with implications for the mixing of air in the bottom of the crater with air on the surrounding plateau [see also Rafkin et al., 2014; Tyler & Barnes, 2013]. The planetary boundary layer (PBL) in Gale Crater may be particularly suppressed in comparison with other locations on Mars, with significant impact on the observations of trace gases made by MSL/SAM (Moores et al., 2019; Newman et al., 2017; Rafkin et al., 2016).

2.2.2. ChemCam Passive Sky Observations

Although the MSL ChemCam spectrometer was designed primarily for laser-induced breakdown spectroscopy (LIBS) of Martian surface materials (Maurice et al., 2012; Wiens et al., 2012), it can also operate in "passive" mode to observe solar radiation scattered by the surface and atmosphere. The ChemCam passive mode was initially used only for reflectance spectroscopy of surface materials (Johnson et al., 2015). However, routine ChemCam passive sky spectroscopy started on sol 230 and McConnochie et al. (2017a) has used these observations to derive aerosol properties and water vapor column abundances using the instrument's visible and near-infrared (VNIR) spectral band. ChemCam also observes O_2 absorption near
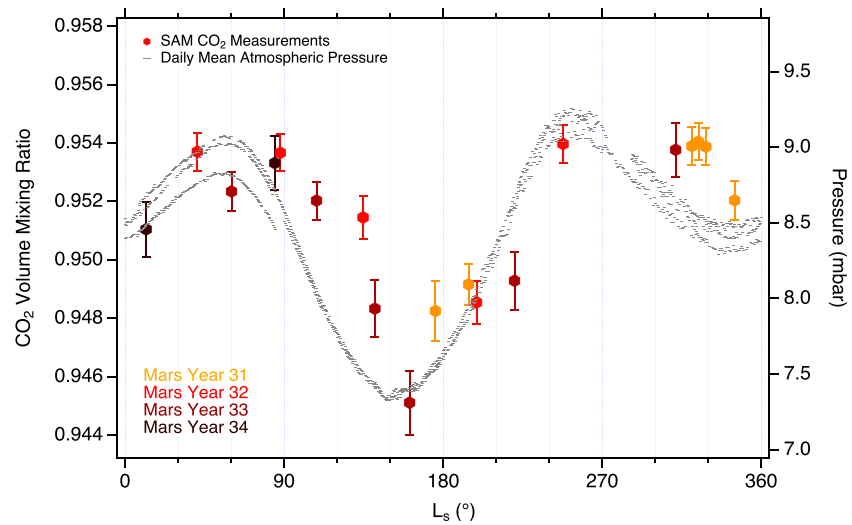
Figure 5. SAM measurements of the CO_2 volume mixing ratio (symbols, left axis). The color scale is matched to Mars year, with tones going from lighter to darker as the points move from Mars year 31 to 34. The error bars on individual points are derived from the uncertainties on the trace gas measurements as described in the text. The daily mean pressure at the surface pressure (gray dashes, right axis), indicating the general pressure cycle on Mars. The vertical axes are set so that the minimum and maximum points in each data set are aligned allowing for visual comparison of the trends. An average CO_2 mixing ratio of 95.1% $\pm$ 0.3% is derived from these data.

762 nm (McConnochie et al., 2017a), and preliminary results (McConnochie et al., 2017b) indicate that this can be used to derive quantitative O_2 column abundances, pending further work to better characterize measurement uncertainties. Because the ChemCam passive sky data are taken at a higher frequency and lower precision than the SAM QMS mixing ratios, they may be able to provide a complementary measurement to track the seasonal behavior of molecular oxygen in and above Gale Crater. Future reports from the ChemCam passive sky measurements may prove valuable for the interpretation of the SAM O_2 mixing ratios.

3. Results: In situ Volume Mixing Ratios

3.1. Carbon Dioxide (CO_2)

Carbon dioxide is the primary component of the Martian atmosphere, with large seasonal variations in the global surface density due to the condensation and sublimation of CO_2 in the polar regions during winter and spring, respectively. This was first observed by the Viking landers through global fluctuations of about 30% in surface pressure (e.g., Tillman et al., 1993). Curiosity pressure measurements to date have shown this cycle as well (Haberle et al., 2014; Harri et al., 2014). The Curiosity landing and science investigations commenced shortly after the annual pressure minimum, which corresponds with the formation of the larger southern polar cap (Figure 1). During the first 200 sols of the mission, the average surface pressure rose steadily to the annual maximum during northern fall, shortly after perihelion. The pressure then decreased to a local minimum near MSL sol 470 during the formation of the north polar cap, which begins to sublime again during the northern spring. The pressure was observed to decrease again as the southern seasonal polar cap was formed, repeating the annual cycle as observed in Gale Crater. SAM QMS measurements after MSL sol 680 have been timed to check for interannual repeatability and to achieve reasonable coverage over the pressure curve.

The SAM measurements are the first comprehensive compositional measurements of the atmosphere taken at intervals throughout Mars' CO_2 cycle. Figure 5 shows the local VMR values determined through MSL sol 1869 (MY 34, L_S 85°) as a function of solar longitude, with the daily average pressure included for comparison to the global cycle. Tabulated data are given in Table S1 and are publicly available (Trainer, 2019a, 2019b). Although there are large fluctuations in CO_2 VMR driven by seasonal and diurnal cycles, CO_2 is so dominant that the volume mixing ratio only varies by 1% about a computed average mixing ratio of 0.951 $\pm$ 0.003.
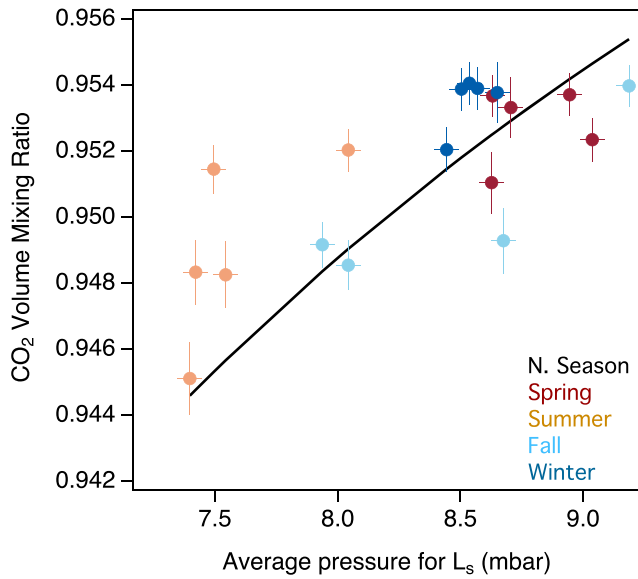
Figure 6. The SAM-measured CO_2 volume mixing ratios (filled symbols) are plotted against the average pressure for the L_S on which the data point was taken, based on approximately 2 years of data taken by the REMS pressure sensor. The colors indicate the time of year: N. spring (Ls 0°–90°), N. summer (90°–180°), N. fall (180°–270°), and N. winter (270°–360°). The expected value for the CO_2 mixing ratio, based on constant composition, is shown as the solid black line.

The small seasonal perturbation (~1%) in the measured VMR is related to, but does not strictly follow, the surface pressure cycle. The decrease of the relative amount of CO_2 in the atmosphere shows a lag behind the decrease of the average surface pressure by roughly 20–40° of L_S during the northern summer as the pressure approaches the annual minimum. The data are sparser during the northern winter, but a similar lag is also indicated as the pressure approaches the seasonal minimum. The hemisphere-to-hemisphere redistribution of mass that occurs during these periods of cap sublimation and condensation pulls atmospheric components toward the winter pole. Transport acts very rapidly to maintain pressure equilibrium, but changes in VMRs lag behind because physical mixing of air masses is a slower process.

To better characterize the mixing process, we introduce an annual-mean VMR (VMR') that differs from the instantaneously measured VMR by a simple correction factor. The simplest scenario (although inaccurate because the mixing timescale is not as fast as the transport timescale) is that composition and total pressure at a specific location on Mars adjust simultaneously, as CO_2 condenses/sublimes in polar regions, while other species remain in the gas phase. If this simple scenario held, then composition and total pressure could be related by the equation:

$$P_{atm}(t) = \sum P_i + P_{CO2}(t) = \sum P_i + P_{CO2(avg)} + dP_{CO2}(t), \quad (4)$$

where $P_{atm}(t)$ is the total atmospheric pressure as a function of time of year; P_i is the partial pressures of the long-lived, noncondensable species; $P_{CO2(avg)}$ is the average annual partial pressure of CO_2; and $dP_{CO2}(t)$ is the variation in the partial pressure of CO_2 as a function of the time of year. The total average annual pressure of the atmosphere ($P_{atm(avg)}$) is then the sum of the partial pressures of the total noncondensable species and $P_{CO2(avg)}$. The value of $P_{atm(avg)}$ for Gale Crater was determined by fitting multiyear daily mean pressure measurements from the REMS data, binned by integer L_S values to provide a seasonally averaged pressure. The average pressure computed in this way is 8.46 mbar. The average CO_2 VMR is used to determine the values for $P_{CO2(avg)} = 8.05$ mbar and $\sum P_i = 0.41$ mbar. The $P_{atm}(t)$ term was fit to a polynomial and a correction factor (F_P) developed to allow the measured VMR values for the noncondensable species to be adjusted to the annual average volume mixing ratio, VMR':

$$VMR' = F_P \cdot VMR. \quad (5)$$

The details of the pressure fit, this calculation, and the derived F_p values are provided in Figure S2.

Similarly, in the (unrealistic) fast-mixing case, $P_{CO2}(t)$ and $P_{atm}(t)$ should be linearly related. This scenario is plotted as VMR versus P_{atm} in Figure 6, where the expected relationship is represented by the black curve, and measured values are shown with symbols. The expected value for the CO_2 mixing ratio was calculated by subtracting $\sum P_i = 0.41$ mbar from the daily mean pressure at the same L_S of the measurement and dividing the $P_{atm}(t)$ to get the mixing ratio (equation (4)). The SAM CO_2 VMR data show a deviation from this relation, in particular the seasons containing the pressure minima. (N. summer and winter) show consistent enhancements above the fast-mixing relation. In the periods during which the seasonal caps are subliming, the measured CO_2 mixing ratio is more likely to match or run below the fast-mixing relation, as can also be seen in Figure 5. By comparing the actual data with the fast-mixing relation in Figure 6, we calculate a correlation coefficient of $R^2 = 0.36$. This poor correlation indicates that the fast-mixing model does not adequately match the observations.
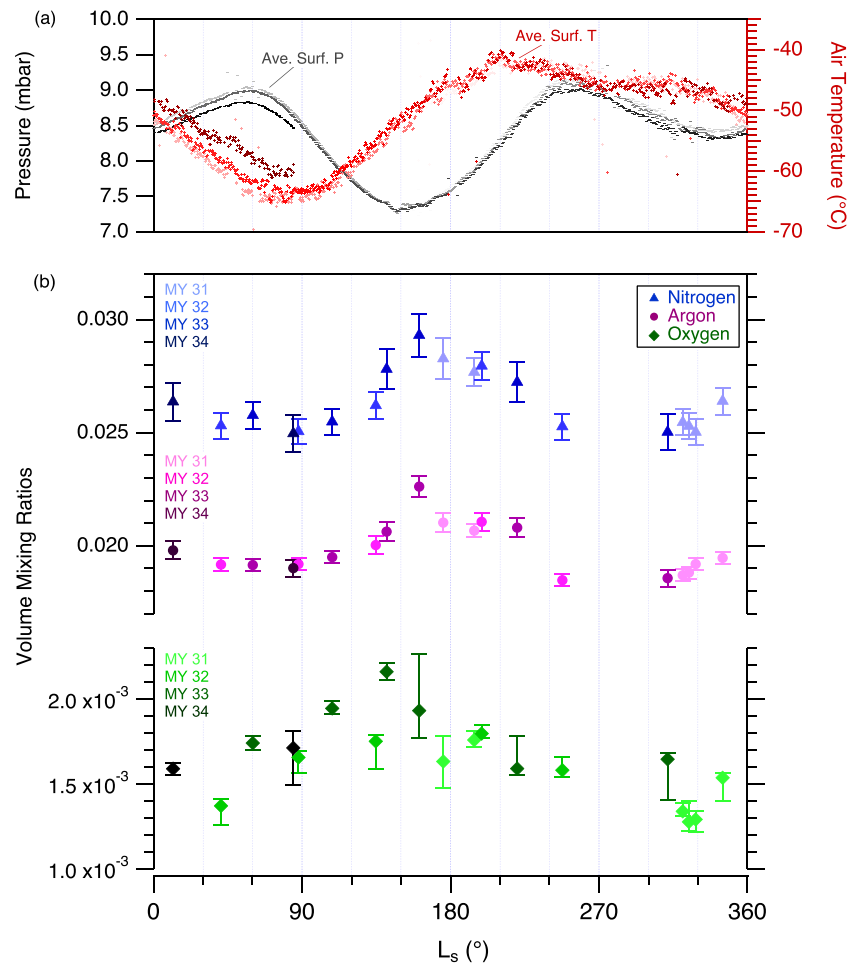
The seasonal fluctuations of the atmospheric pressure, and the influences of dynamics on the atmospheric composition at this location on Mars, are more easily identified and understood by studying the behavior of the trace, noncondensable components, which are more sensitive to the changes in global pressure. These are discussed in the next section.

Figure 7. Seasonal trends in the instantaneous volume mixing ratios of the three most abundant noncondensable gases in the Mars atmosphere show a general inverse relationship with pressure due to the condensation and sublimation of CO_2 from the polar deposits. **(a)** Daily mean atmospheric pressure (gray dashes, left axis) and air temperature (red dashes, right axis) show the environmental conditions in Gale Crater as influenced by the seasonal cycle on Mars. Darkest points are the most recent. **(b)** Nitrogen (triangles), argon (circles), and oxygen (diamonds) are plotted versus. L_S. Point shading corresponds with Mars year (light to dark) as indicated in the upper left corner of each plot. Error bars shown are 1-σ, computed as described in section 2.1.1. All plotted data are publicly available (Trainer, 2019a, 2019b).

3.2. Noncondensable Atmospheric Components

The mixing ratios of argon (^{40}Ar), nitrogen (N_2), and oxygen (O_2) are shown in Figure 7, and carbon monoxide (CO) is shown in Figure 8. These next four most abundant species are not condensable at Mars surface and atmospheric temperatures and pressures and thus are not expected to deposit or sublime from the polar caps as does CO_2. However, there are seasonal trends in the VMR of these molecules that are a response to mixing of air masses during the seasonal CO_2 cycle and unexplained additional processes affecting O_2 and CO.

For reference, Table 2 provides instantaneous volume mixing ratios for these gases measured by MSL/SAM at approximately the same time of the Mars year as the Viking landers. The previous in situ measurements were not operational for the full Mars seasonal cycle.

3.2.1. Argon and Nitrogen

Argon and nitrogen serve as excellent tracers of global transport, since they are chemically inert in addition to remain solely in the gas phase. Figure 7b shows that, as expected, these two species track each other consistently through the Mars year, with good year-to-year repeatability. Instantaneous composition is plotted (i.e., VMR as opposed to VMR′). Pressure maxima occur near L_S 60° and 250°, after the seasonal
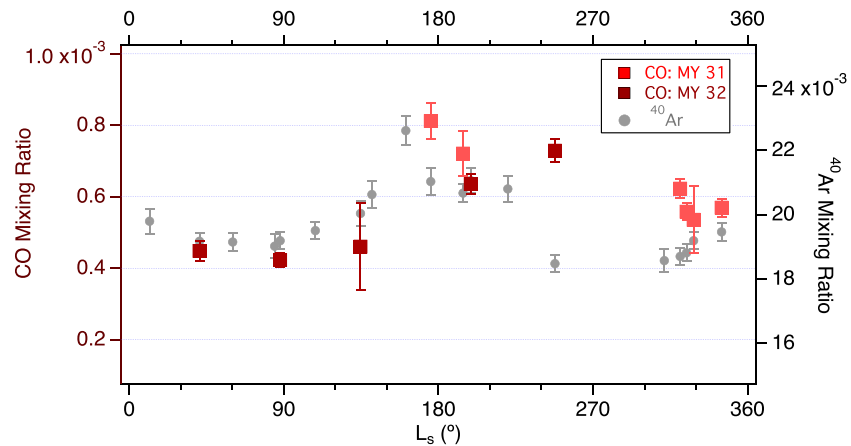
Figure 8. The CO measurements for the first 830 sol (shaded by Mars year) appear to follow the general trend of Ar, particularly in the spring through summer. Data after mission sol 1,000 show substantially elevated signal at m/z 12, and the derived mixing ratios are consistently high with no apparent seasonal modulation. These data are not reported in this publication.

northern and southern polar caps (respectively) have sublimated. Minima in Ar and N_2 VMRs lag behind these pressure maxima by ~30° L_S, suggesting a slower mixing timescale (although the timing of the northern winter minima in Ar and N_2 VMRs are poorly constrained by the SAM QMS data, we assume the minimum is at L_S 280°). The lag between pressure minima and VMR maxima (~15° L_S) is much smaller than the lag between pressure maxima and VMR minima (~30° L_S), but note that VMR′ is better suited to compare global transport and mixing timescales. The VMR data are provided in Figure 11 with a detailed discussion in section 4.1.

The four right-most points in Figure 7b for both Ar and N_2 show the time period in MY 31 during which daytime and nighttime measurements were taken within close proximity. From left to right, this group of points represents: day–night–night–day (Table 1). Although there appears to be a change in the mixing ratio among these points, there does not appear an obvious correlation with time of day.

N_2 and ^{40}Ar have mean mixing ratios of approximately 2.6% and 1.9%, respectively, with a seasonal variation of ±10% of these values throughout the year (Table 3). Note that the temporal average reported here is affected by limited number of samples (Figure 1); we use a strict numerical average without regard to temporal coverage. The nitrogen mixing ratio has been increased substantially (Franz et al., 2017) from the originally published value in Mahaffy et al. (2013) and is now consistent with the Viking values within the uncertainty of those previous measurements. A detailed discussion of the updated calibration constants for the SAM QMS and the adjusted mixing ratios for the first sols of the SAM QMS measurements is given in Franz et al. (2017), which included corrections based on a calibration cell experiment on Mars.

Table 2
Viking and SAM Mixing Ratio Values for Similar Seasonal Periods

	Viking GCMS[a]	MSL SAM	Viking GEX[b]	MSL SAM
L_S (°)	100	108	121 – 142	134,141[c]
CO_2	95.32%	95.2% ± 0.1%	96.2% ± 5%	95.0% ± 0.2%
N_2	2.7% ± 0.5%	2.55% ± 0.06%	2.3% ± 0.3%	2.70% ± 0.11%
^{40}Ar	1.6% ± 0.3%	1.95% ± 0.03%	1.5% ± 0.3%	2.03% ± 0.06%
O_2	1300 ± 260 ppmv	1940 ± 40 ppmv	<1500 ppmv	1950 ± 290 ppmv[d]

[a]Owen et al., 1977 (±20% uncertainty on values were prefinal calibration estimates, as stated in their text, and O_2 might be based on earlier ground-based observations (see discussion in section 4.2 here)).   [b]Oyama & Berdahl, 1977. [c]Average of two measurements taken at these L_S values. Local "instantaneous" mixing ratio is increasing during this time.   [d]Oxygen exhibits large interannual variability in the MSL/SAM data set, reflected in the uncertainty on this average.

Table 3
Annual Mean Volume Mixing Ratios for Mars Atmosphere [a]

Atmospheric component	Annual mean mixing ratio	Uncertainty on mean[b]	Seasonal variation from mean	Approximate measurement error[c]
CO_2	0.951	± 0.003	1%	2.9%
N_2	0.0259	± 0.0006	10%	3.2%
Ar	0.0194	± 0.0004	9.7%	2.0%
O_2	0.00161	$\pm 9 \times 10^{-5}$	13%	18%
CO [d]	0.00058	$\pm 8 \times 10^{-5}$	36%	6.1%

[a]Corrected for annual mean pressure ($\times P/P_0$; using equation (5)), except for CO_2. P is the annual mean pressure in Gale Crater, 8.46 mbar. [b]Uncertainty on the annual mean mixing ratio is reported as 2× the standard deviation of the mean. [c]Typical uncertainty on the individual instantaneous measurements for each atmospheric component. [d]Reflects measurements from the first 830 sol only; see discussion in section 3.2.3. This likely skews the mean value toward northern winter (36% of measurements; Figure 8).

The $^{40}Ar/^{14}N$ ratio of the Mars atmosphere, in combination with $^{14}N/^{15}N$, has been used as a diagnostic tool for verifying the inclusion of trapped atmosphere in Martian meteorites, as it has a unique signature as compared to Earth (Becker & Pepin, 1984). This has been discussed previously in the context of the SAM $^{14}N/^{15}N$ measurements (Wong, Atreya, et al., 2013), but the value has been updated with the new SAM calibration (Franz et al., 2017). The $^{40}Ar/^{14}N$ ratio also serves as a useful metric by which to evaluate the robustness of the mixing ratio measurements of these trace gases over time. The relative abundance of these two gases should remain constant, since neither is expected to react or condense, and their similar abundances ensure near-identical transport during the seasonal cycle on Mars. The $^{40}Ar/^{14}N$ measured by SAM throughout the mission is shown in Figure 9 as a function of MSL sol and indeed shows multiyear consistency within measurement uncertainty, with an average value of 0.376 ± 0.008.

3.2.2. Oxygen

The measured mixing ratio of O_2 has varied from approximately 1,300 to 2,200 ppmv during MSL's first 1,900 sols at Gale Crater (Figure 7b). Two unexpected features of the seasonal behavior of O_2 are immediately apparent when comparing to the other major inert species (Figure 7b). First, O_2 does not follow the same general pattern as the Ar and N_2, particularly through the beginning of the year. Second, the O_2 mixing ratio shows substantial interannual variability. Both of these features are surprising, because the chemical lifetime of Martian atmospheric O_2 is estimated to be ≥ 10 Earth years (Krasnopolsky, 2017). Like Ar and N_2, O_2 does not condense under Mars atmospheric conditions, so the $O_2/^{40}Ar$ ratio is expected to be constant, as for the Ar and N_2. Despite the larger uncertainties on the derived O_2 mixing ratios (section 2.1.1), two prominent seasonal features are apparent in the O_2 VMR data (Figure 7b) and the $O_2/^{40}Ar$ ratio (Figure 10): There is a gradual northern spring/summer increase in O_2, followed by a potentially rapid reset to a constant level over much of northern summer and fall (L_S 160°–315°).

The spring/summer increase in O_2 can only be characterized in a broad sense, due to the large error bars and coarse sampling of the time series. If we make the simplest assumption, a linear change in VMR as a function of L_S in the L_S 0°–150° period, there is almost a factor of 3 variation in rate of change in MY 32, MY 33, and MY 34 (from about 1.3 to 3.6 ppm/°L_S; Figure 7b). The VMR values plotted in the figure include the effects of both seasonal CO_2 condensation/sublimation and global mixing. By instead considering the $O_2/^{40}Ar$ ratio (Figure 10), we can eliminate all changes due to condensation/sublimation and global mixing, and it becomes more reasonable to apply a constant rate of change to all 3 years of O_2 observations. Any remaining changes in the $O_2/^{40}Ar$ ratio indicate other factors controlling the local mixing ratio of oxygen in Gale Crater besides the large-scale global dynamics controlling transport during the seasonal cycle. We will discuss this result in more detail below in section 4.2. A significant change is clear over the L_S 0°–150° period, with a consistent rate of 0.012%–0.015% /°L_S. The exact onset and end of the O_2 increase season are not well defined, and the data are not finely sampled enough to determine whether the increase is truly linear (or whether there is variation year to year).
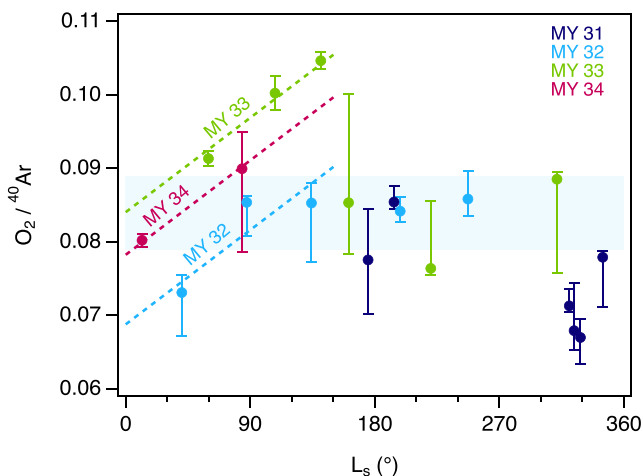
The second O_2 seasonal feature is that $O_2/^{40}Ar$ mixing ratios (Figure 10) are more or less constant and identical in all Mars years, over the period of L_S 160°–315°. During this part of northern summer and fall,
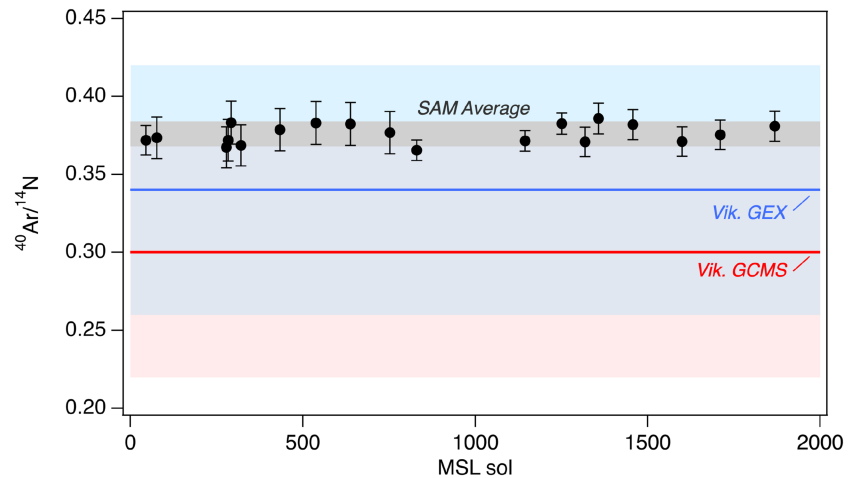
Figure 9. The $^{40}Ar/^{14}N$ ratio is consistent over the course of the mission within the measurement uncertainties, verifying the robustness of the mixing ratio measurements during nearly 5 years on Mars. The SAM $^{40}Ar/^{14}N$ is greater than the values reported by Viking instruments (GCMS, red line; GEX, blue line) but is within the range of uncertainties, as indicated by the red- and blue-shaded regions. SAM has measured a larger proportion of Ar in the atmosphere than the previous landed instruments. Small perturbations in this ratio correlated to local air temperature are discussed in Figure S9.

the $O_2/^{40}Ar$ mixing ratio is identical to the annual mean of 0.083 (within uncertainties). It is important to note that the sparse temporal sampling of the data is not sufficient to precisely characterize the bounds of this constant period. However, MY 33 data on L_S 141° and 161° show a rapid decrease of 20%–25% in $O_2/^{40}Ar$. This is a remarkably rapid change, potentially giving insight into the processes modifying atmospheric O_2 abundances, though we note that the rapid decrease was only observed during MY 33.

Finally, interannual variation is clearly apparent from offsets between measurements in the spring/summer season of increasing $O_2/^{40}Ar$ mixing ratio. Full characterization of the interannual variation is not possible given the sparse temporal sampling, but the onset of the variable period seems to be sometime later than L_S 270° and sometime earlier than L_S 30°.

We investigated the possibility of instrument effects or other measurement artifacts affecting the retrieval of the O_2 mixing ratio and thus contributing to the apparent variability. As noted in section 2.1.1, the O_2 mixing ratio is computed based on the signal at m/z 32, which has both a high background signal and a contribution from the fragmentation of $CO_2{}^+$. The backgrounds and corrections have been tracked through the course of the mission, and we have found no correlation with the increases in both absolute and relative O_2 mixing ratios. Further, the O_2 measurements were checked against the solid sample analyses to determine whether there could be contamination from a pyrolysis experiment. There was no unique correspondence between solid samples with O_2 release and large increases in the atmospheric O_2 mixing ratio or background measurement (Figure S4).

3.2.3. Carbon Monoxide

Carbon monoxide (CO) has been detected and is quantified as reported in Franz et al. (2017, 2015). As discussed in those publications and in Mahaffy et al. (2013), the quantification of CO relies on a marginal detection above the dominant CO_2 component, which generates CO^+ and other interfering fragments in the QMS. Even when the CO abundance was measured at a relatively high value (i.e., near L_S 180°, TID 25012), the signal at m/z 12 is estimated to be comprised of 15% directly ionized CO and

Figure 10. The $O_2/^{40}Ar$ ratio, plotted against L_S and shaded by Mars year, highlights the variability in O_2 that exists outside global seasonal transport. The light blue-shaded region shows the overlapping mean and median of the data set, an $O_2/^{40}Ar$ of 0.083 (±5%). Dashed lines show fits to the data in the L_S 0°–150° range, under a simple linear model that fits a single slope to all the data, but separate intercepts for each Mars year.

85% from CO_2 fragmenting into CO^+. The derived CO mixing ratios for the first part of the mission are given in Figure 8. It can be seen that these species approximately track the seasonal trend in argon, behaving much like a passive tracer species through the atmosphere. This is generally what is assumed in photochemical models, although there has been some observational variability that has challenged this assumption [see discussion in Krasnopolsky, 2015]. Smith et al. (2017) recently published CRISM column observations of CO for MY 28 through MY 33, therefore overlapping in the time period of the reported MSL measurements. The CO derived from CRISM data for the latitude band at 0°–20°S shows a similar trend, with a minimum at L_S 90° and a subsequent rise to a peak value just before L_S 180°. The absolute value of the mixing ratio measured by SAM ranges from 400 ppm to 800 ppm during this period, which is slightly lower than the 700–1000 ppm reported by CRISM for this region on Mars. Other orbital and ground-based measurements also report greater CO mixing ratios than the in situ values (Billebaud et al., 2009; Encrenaz et al., 2006; Hartogh, Błęcka, et al., 2010; Krasnopolsky, 2003, 2015; Sindoni et al., 2011; Smith et al., 2009). There are several possible explanations for any discrepancy between the surface and the orbital and ground-based observations, including the difference in spatial sampling, the effect of any local depletions in Gale Crater, errors in the SAM CO measurement, and the distinction between a point and column-integrated measurement.

Although we have measured the CO in each atmospheric experiment through MSL sol 1,711, measurements after sol 1,000 show significantly elevated signal at m/z 12 and therefore very high CO mixing ratios. The VMR for CO obtained in MY 32, near L_S 250° (MSL sol 830, TID 25232, Tables 1 and S1) shows the onset of this trend, in which the CO begins to diverge from the repeated seasonal trend in Ar (Figure 8). In addition to the derived CO mixing ratio, more than doubling from MY 32 to MY 33, the elevated measurements have not decreased or shown any seasonal modulation in MY 33 and MY 34, in contrast to the O_2 measurement. This behavior is suspect, and at this time, a possible contamination or instrument effect cannot be ruled out. Especially because we know the m/z 12 signal to be highly sensitive to such effects (Franz et al., 2015), we are cautiously omitting the questionable observations from this paper. Those CO measurements thus require further investigation and will be reported at a later time.

4. Discussion

4.1. Seasonal Transport

Argon and nitrogen in Mars atmosphere have extremely long lifetimes (~Gyr) against losses from photochemistry, sputtering, and escape, and they do not condense under any of the conditions reached during the current seasonal cycle. Condensation points at Mars ambient pressures are ~63 and 53 K for Ar and N_2, respectively. Thus, these gases serve as excellent tracers of the complicated dynamics induced by the cycling of CO_2 into and out of the polar caps on yearly timescales. Measurements of Ar from orbit using gamma subsystem (GS) of the gamma ray spectrometer (GRS) on the Mars Odyssey spacecraft first identified a "freeze distillation" effect, in which Ar (and other noncondensables) are carried to the polar regions by advection of the bulk atmosphere during autumn and winter when CO_2 freezes out on the polar cap (Sprague et al., 2007). The GRS measurements provide a column-averaged mean mixing ratio (mmr) of Ar relative to the total atmospheric gas and show an enrichment of up to 6 times at the southern winter pole and 3 times at the northern winter pole (Lian et al., 2012; Sprague et al., 2012). However, the orbital measurements of Ar at the lower latitudes have too much scatter to detect what could be seasonal variations of a smaller magnitude (Sprague et al., 2012).

Recently published work from the alpha particle X-ray spectrometer (APXS) on the Mars Exploration Rover Opportunity (MER-B) has reported a relative atmospheric argon density over 6 years of observation from ~2°S, a similar latitude as MSL (VanBommel et al., 2018). The MER-B measurements, from Mars years 28–33, provide normalized argon mixing ratios that show a seasonal variation of up to 15% from L_S 0°, which is comparable in magnitude to the observed variation in absolute mixing ratios measured by SAM, with broadly similar seasonal trends. More detailed analysis, beyond the scope of this paper, will be needed to assess the statistical and physical significance of the modest differences between SAM and APXS. Note however that the spatial separation of MER-B and MSL and the much larger volume of atmosphere sampled by the APXS detection method could contribute to such differences due to the significance of atmospheric dynamics in mixing ratio trends.
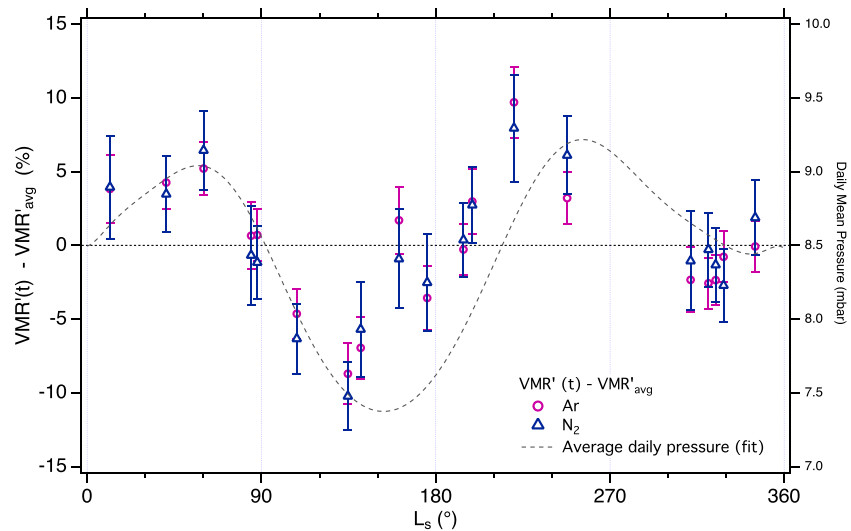
Figure 11. The global annual mean values of Ar and N_2 (Figure S5) were subtracted from the pressure-corrected mixing ratios of Ar and N_2 (VMR′, equation (5)) at each seasonal point and plotted as a percent deviation from the average. In this way, the observed seasonal cycle of Ar and N_2 can be compared directly to a flat annual mean that removes the mixing ratio changes introduced by fluctuating CO_2 pressures. If there were no influence of transport, the corrected VMR′ values would appear on the dashed zero line. The polynomial fit to the daily mean pressure data is shown as a gray dashed line for comparison to the annual pressure cycle.

With SAM QMS measurements, we have the first data set of compositional measurements near the equator of all the major species, thus painting a more complete picture of the behavior of Mars' atmosphere throughout the seasonal cycle. The instantaneous mixing ratio data presented in Figure 7 and Table S1 were subsequently adjusted for the annual global pressure cycle, using the method described in section 3.1. We used equation (5) to correct the in situ values to produce global mean annual mixing ratios (VMR′, Figure S5). If the atmospheric gases were perfectly globally mixed and transport effects on trace species were negligible at this low latitude, the amount of Ar and N_2 would show a constant value once the pressure variation was removed. In other words, the Ar and N_2 VMR′ values in Gale Crater would remain constant with time, if atmospheric transport and mixing timescales were identical. The corrected mixing values (Figure 11) show that there are clear deviations to such behavior, because the transport (traced by adjustment of atmospheric pressure due to polar CO_2 condensation/sublimation) is faster than mixing (traced by adjustment of composition). Global mean values were calculated from the Ar and N_2 VMR′ (0.0194 and 0.0259, respectively), about which the individual mixing ratios are plotted. In this manner, the two atmospheric components can be plotted on the same axis, highlighting deviations from the average value as a function of L_S. The data indicate that the minimum in Ar and N_2 VMR′ in N. spring/summer lags behind the pressure maximum by approximately 78° of L_S, and similarly the maximum in Ar and N_2 in N. summer/fall follows the pressure minimum by 67° of L_S, due to delay in mixing.

The corrected mixing ratios indicate mixing of air masses of distinct composition, moving through the equator during the seasonal cycle. At the south pole, maximum enrichment of Ar observed at the southern pole by the GRS (Sprague et al., 2012) occurs near L_S 120°, an effect of "freeze distillation" of trace gases occurring at the pole during the local winter (Lian et al., 2012). Although pressure at all latitudes adjusts relatively and rapidly to polar sublimation/condensation, compositional differences can be maintained longer by the southern polar vortex until it mixes with higher latitude air in southern spring, pushed by the large amounts of CO_2 subliming off the cap. Repeating cycles of enrichment and depletion of Ar and N_2 are observed at Gale Crater as the composition mixes between low latitude air masses and seasonally varying polar air masses. It should be noted that the orbital GRS measurements of Ar at low latitudes (where both Opportunity and Curiosity sit), and even in north polar regions, are dominated by scatter and the variations described here are not resolvable.

Differences in the timescales for atmospheric transport and mixing are emphasized by plotting global mean values (VMR′; Figure 11) using the pressure correction described above, since VMR′ should not change if
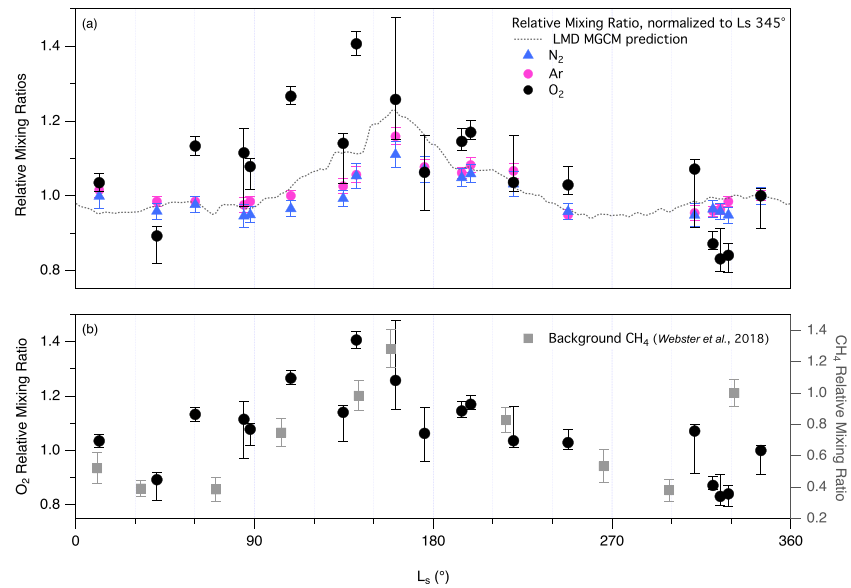
Figure 12. (a) The instantaneous mixing ratios of N_2, Ar, and O_2 (Figure 7, Table S1) are normalized to their values at MY 31, Ls 344.9°, and plotted on top of the MGCM output for relative Ar mixing ratio within Gale Crater. Similar models have produced seasonal variations in Ar at low latitudes that are on the same scale ($\pm$10%) (Lian et al., 2012). (b) The background seasonal CH_4 abundance reported in Webster et al. (2018) is shown here as the instantaneous mixing ratio (right axis), normalized to L_S 330° (MY 32), which allows for comparison to the O_2 measurements (left axis, replotted as in the top panel). Correlations between CH_4 and O_2 are addressed in section 4.2.2.

transport and mixing timescales are identical. We use pressure-corrected VMR′ data to compute mean annual mixing ratios (Table 3), but as indicated by the residuals plotted in Figure S5, uncertainties in the global average are affected more by seasonal variation than by instrumental uncertainties. In Figure 12, we plot the instantaneous VMR of Ar and N_2 on top of a modeled Ar mixing ratio in Gale Crater as predicted by the Laboratoire de Météorologie Dynamique (LMD) Mars GCM (MGCM) with coupled photochemistry (Lefevre et al., 2004). All are normalized to L_S 345°, selected as one of the SAM measurement points closest to L_S 0° (360°). The MGCM prediction shows generally good agreement with the measured mixing ratios for Ar and N_2, with some discrepancy between L_S 90° and180° when a lower mixing ratio is observed by SAM. The discrepancy between the model and the data may reflect an inaccurate estimation of the local isolation in Gale Crater that limits mixing between the MSL measurement sites and the surrounding atmosphere (Pla-Garcia et al., 2016; Rafkin et al., 2016). Thus, the SAM data set provides unprecedented ground truth measurements of these tracers to aid in improving the representation of various processes within the Martian climate system in global circulation models. This has significant implications for proper understanding of the water cycle, CH_4 abundance and distribution (Webster et al., 2018), and possibly also the dust cycle on Mars (Lian et al., 2012).

MER-B used APXS data to measure seasonal trends in Ar mixing ratio at Meridiani Planum. General trends are very consistent with SAM results at Gale Crater (Figure 7), but the cadence of the SAM data preclude a definitive observation of the argon "pulse" near L_S 150° observed in the APXS data [see Figure 9 in VanBommel et al., 2018]. The SAM data are not inconsistent with a pulse; qualitatively, in particular with the pressure-corrected data (Figure 11), there appears to be a small increase in Ar around L_S 150° that deviates from an apparent seasonal curve. Interestingly, L_S 150° also corresponds to the timing of the transition between seasonal periods of increasing O_2 and constant O_2 in the SAM data set (section 3.2.2).

4.1.1. Nitrogen Cycle

Recent detections of nitrate in Martian sediments have indicated the presence of nitrogen fixation cycles on Mars at least at one time in its history (Navarro-Gonzalez et al., 2019; Stern et al., 2015; Stern et al., 2017). Because nitrogen is an essential element for life, nitrogen fixation is a critical process required to support habitable environments as we know them. If currently active, a large nitrogen flux into the regolith could potentially affect the abundance of atmospheric N_2 over seasonal or long-term timescales. We explored

whether the available SAM atmospheric data set could shed any light on whether there is a currently active nitrogen cycle. As on Earth, the primary reservoir of nitrogen is in the form of N_2 in the atmosphere. On Earth, nitrogen fixation proceeds abiotically and biologically, with the biological rate (10^{14} g N yr^{-1}) occurring about 100 times higher than the abiotic rate triggered by lightning (Menge et al., 2013; Schumann & Huntrieser, 2007; Zehr et al., 2001). Nitrogen-containing end products of biological processes are rapidly recycled back into the atmosphere at a rate such that the nitrogen budget on Earth appears to be in an approximate equilibrium. On Mars, nitrogen fixation could potentially occur both biologically (Klingler et al., 1989) and abiotically (Navarro-Gonzalez et al., 1998; Navarro-Gonzalez et al., 2001; Segura & Navarro-Gonzalez, 2005). Currently there exist no data capable of providing evidence of biological activity on Mars. If reported, CH_4 detections (Formisano et al., 2004; Mumma et al., 2009; Webster et al., 2013; Webster et al., 2015; Webster et al., 2018) were assumed to be solely a result of active biological activity; an estimated biomass of ~10^9 g yr^{-1} would be required to maintain a CH_4 concentration of 10 ppbv (Krasnopolsky et al., 2004). A methanogenic population of this size would be capable of a hypothetical biological nitrogen fixation rate of ~10^8 g N yr^{-1} (Frigstad et al., 2011; Leigh, 2000). Conversely, photochemical models predict an abiotic nitrogen fixation rate of ~10^9 g N yr^{-1} in the form of nitrates (Yung et al., 1977). Therefore, the abiotic rate in the current atmosphere would be expected to exceed the hypothetical biological rate by at least an order of magnitude. The current annual flow of nitrogen from the atmosphere to the surface is negligible considering a repository in the atmosphere on the order of 10^{18} g N_2.

Further, the abiotic denitrification of nitrates is a viable mechanism to recycle back surface nitrogen to the atmosphere, but the rate of this process is currently unknown. Therefore, it is concluded that current nitrogen cycle on Mars has no measurable impact on the atmospheric N_2 mixing ratio and consequently implies nitrogen seasonal stability.

4.2. Oxygen
4.2.1. Interannual Variability
The 1300–2200 ppmv abundances of oxygen measured by SAM are generally in the same range as prior measurements that span different sets of in situ and remote sensing observations of O_2 in the upper atmosphere and at the surface of Mars. The repeated measurements of SAM provide the most robust measurements to date, as the previously reported values have been made with substantial uncertainty and limited frequency, besides being in different regions of the atmosphere and the surface. From five sets of mass spectral measurements obtained within days of landing of Viking lander 1 (VL1) on 20 July 1976, Owen and Biemann (1976) reported an O_2 mixing ratio in the 1000–4000 ppmv range. Owen et al. (1977) subsequently concluded that the oxygen measurements had considerable scatter of a factor of 2, which they attributed to instrumental causes. It seems likely, as England and Hrubes (2004) suggest, that Owen et al. (1977) based the 1300 ppmv value for O_2 mixing ratio given in their Table 1 on measurements reported by Barker (1972) and Carleton and Traub (1972), which were obtained with high-resolution 762 nm O_2-band spectroscopy from terrestrial observatories (see also Trauger & Lunine, 1983 who report a slightly lower value from ground-based spectroscopy: ~1200 ppm when scaled to 6 mbar surface pressure). The Viking GEx experiment reported an *upper limit* of 1500 ppmv (Oyama & Berdahl, 1977). England and Hrubes (2004) calculated a seasonal variation in O_2 between 2,500 and 3,300 ppmv, by inverse scaling of O_2 to atmospheric pressure measured by the Viking. It is important to note that the reference O_2 value they used in their scaling calculation (3,000 ppmv) is the value VL1 measured at 125–300 km, in the upper atmosphere above the homopause (Nier & McElroy, 1977), which is not representative of O_2 at the surface. Mars Express SPICAM observed 4,000 ppmv O_2 averaged over 90–130 km and six observations (Montmessin et al., 2017; Sandel et al., 2015). Any seasonal or temporal variations in O_2 at the surface are not expected to propagate to the upper atmosphere. Recent measurements made through disk-averaged observations of Mars with the Herschel Space Observatory's HIFI instrument retrieved a value of 1400 ± 120 ppmv, though they caution the reader the value may not be vertically uniform (Hartogh, Jarchow, et al., 2010). This measurement was taken during MY 30, L_S 77°. SAM measurements from surface from similar times of year are slightly higher but with overlapping uncertainty (Table S1).

The SAM measurements of O_2 in Gale Crater do not show the annual stability or seasonal patterns that would be predicted based on the known sources and sinks in the atmosphere. As mentioned in section 3.2.2, based on known sources and sinks, O_2 should show the same seasonal patterns and annual

repeatability as Ar. Given the known chemical cycles, the formation of atmospheric O_2 is controlled primarily by photochemistry of H_2O and CO_2 (e.g., Atreya & Gu, 1994):

$$CO_2 + h\nu \rightarrow CO + O, \tag{R1}$$

$$H_2O + h\nu \rightarrow H + OH, \tag{R2}$$

$$OH + O \rightarrow H + O_2, \tag{R3}$$

and

$$O + O + M \rightarrow O_2 + M, \tag{R4}$$

where M is the background gas (CO_2). The abundance is then controlled by the balance between formation and loss through photolysis and formation of H_2O_2, HO_2, and NO_2 (Krasnopolsky, 1993).

To quantify the enrichment of the observed O_2 compared to what would be predicted, we account for the changes in total number density, which are mainly due to pressure changes (Figure 7a) caused by the global-scale CO_2 condensation-sublimation cycle, as well as the expected changes in the mixing ratios of all noncondensable gases, which are caused by the interaction of the global circulation with that condensation-sublimation cycle and are readily visible to us via Ar results. After accounting for both of these, it can be estimated that approximately 10^{14} O_2 molecules cm^{-3} must be added to the atmosphere sampled by Curiosity in order to explain the observed 1,700 to 2,200 ppmv increase in O_2 between L_S 60° and 140° in MY 33. In other words, the number density of O_2 molecules at L_S 140° in MY 33 is $\sim 10^{14}$ molecules cm^{-3} larger than it would have been had the ratio of O_2 to Ar remained constant as expected. For reference, given the 1,700 ppm starting value at L_S 60°, the O_2 mixing ratio would have been $\sim$1830 ppm at L_S 140°, had the O_2 to Ar ratio remained constant over that time span.

Using the $O_2/^{40}Ar$ ratio as an indicator for O_2 variability outside of the known and observed seasonal dynamics, a simple linear model can be used to fit a single slope to all the data (Figure 10). This model highlights a consistent seasonal increase in $O_2/^{40}Ar$ ratio of 0.014/100° L_S during the L_S 0–150° period, with an interannual variation in the mean $O_2/^{40}Ar$ ratio in this period. For $L_S > 150°$, $O_2/^{40}Ar$ seems to be more or less constant, with no significant interannual variation. The low values at $L_S > 310°$ in MY 31 suggest a possibility of additional interannual variation late in the Mars year, and potentially the onset of the increases is observed through the spring of the following years, but future observations would be needed to confirm this possibility.

Within the uncertainties caused by limited sampling and measurement error, this magnitude appears typical of the unexpected seasonal increase, and so going forward, we will adopt $\sim$400 ppm and $\sim 0^{14}$ molecules cm^{-3} as the amount that needs to be resolved. Assuming that the unexpected O_2 is uniformly mixed in the lower atmosphere, as seems likely for perturbations of this timescale given current assumptions about the eddy diffusion coefficient, the 10^{14} molecules cm^{-3} become 10^{20} molecules cm^{-2} in the atmospheric column (see, e.g., Krasnopolsky, 2010 who adopts 10^7 cm^2 s^{-1} for the eddy diffusion coefficient, which gives a $\sim$2-day characteristic timescale for the bottom scale height of the atmosphere).

Given photochemical schemes above, this 400 ppm of extra O_2 would require a corresponding destruction of CO_2 and H_2O molecules in approximately 170 sol. Considering H_2O alone, $\sim$800 ppm of H_2O would need to be destroyed, which is more than five times larger than the maximum abundance of H_2O measured in and around Gale Crater by REMS (Martínez et al., 2016) and ChemCam (Fig. 111 in McConnochie et al., 2018). Thus, it appears unlikely that the needed O_2 could be produced from the available atmospheric water for any plausible H_2O photolysis or dissociation mechanism. Furthermore, H_2O abundance shows an increase during this time period and no strong correlation with O_2 (Figure S6). Estimates for the production of O from CO_2, using CO_2 photolysis rates for the lower atmosphere of Mars (Table 1 in Wong et al., 2003), indicate that this process is much too slow to generate the observed rise over the short ($\sim$1/2 yr) time period. For completeness, note that photolysis or other dissociation of CO is negligible, and in any case a seasonal removal of $\sim$800 ppm of CO is clearly ruled out by observations (e.g., Smith et al., 2009).

The primary destruction pathways for O_2 are through direct photolysis in the upper atmosphere and reaction with photolysis products of H_2O, HO_2, and CO_2 deeper (Atreya et al., 2006; Lefèvre & Krasnopolsky, 2017; Wong et al., 2003). Even factoring in the effects of dust devils and large dust storms (though no major dust events occurred during the measurement period) (Atreya et al., 2006), the lifetime of O_2 against photochemical destruction in the Mars atmosphere is expected to be at least 10 years, possibly longer (Krasnopolsky, 2010; Lefèvre & Krasnopolsky, 2017). Again using the $O_2/^{40}Ar$ ratio as an indicator for O_2 variability (Figure 10), the SAM measurements in MY 33 show a relative decrease of 23% in a period of 39 days (38 sol). (This is a ~500 ppm absolute O_2 decrease from what would be expected from a constant $O_2/^{40}Ar$ ratio given the starting O2 abundance at L_S 140°.) There is a similar decrease observed from fall to winter of MY 31, although the measurement frequency is such that the period of change appears longer (−20% in 201 sol). In particular, the rapid drop in MY 33 corresponds to a lifetime of 150 days, several orders of magnitude less than the photochemical equilibrium lifetime of ≥10 years. The drop in MY 31 corresponds to a lifetime of ~1000 days, which is still relatively short.

The lack of a known atmospheric source or sink that could explain the apparent behavior of the O_2 in Gale Crater suggests the possibility of a temporary surface reservoir. Previously, Herschel WIFI observations found that the O_2 vertical profile above the surface is not constant with altitude (Hartogh, Jarchow, et al., 2010) and preliminary analysis of the data shows that a surface flux of O_2 may be required to explain the observations (Paul Hartogh, personal communication, 2016). A surface sink has been previously invoked to balance the current redox budget (Zahnle et al., 2008), and the surface is known to harbor a variety of oxidant species (e.g., Lasne et al., 2016 review). In fact, the Viking Gas Exchange experiments found that a significant quantity of O_2 was released whenever soil samples were humidified (Klein, 1978; Oyama & Berdahl, 1977) although these experiments were all done at ~10 °C rather than Mars ambient temperatures.

Deposition of oxygen could occur in the form of more reactive oxidized species, superoxides, hydrogen peroxide (H_2O_2), ozone (O_3), or perchlorates, all of which are assumed to have a higher surface reaction probability (γ) with surface materials than molecular oxygen. It is possible to conceive of an oxygen cycle with the appropriate seasonal and interannual variability if oxygen were effectively converted to these species, deposited into the regolith, and then rereleased due to thermal, chemical, or radiation perturbations.

Perchlorates, found to be prevalent in the surface materials in Gale Crater at 0.03–1 wt% level (Sutter et al., 2017), are very stable. They have also been detected at 0.4–0.6 wt% level in the polar landing site of the Phoenix Lander (Hecht et al., 2009). To put perchlorates in context, a 1-cm depth of soil containing 1% by weight of calcium perchlorate has slightly more than enough oxygen to contribute the apparent ~10^{20} molecules cm^{-2} of unexpected column O_2 variation, and O_2 has been shown to be a high yield product of radiolysis of surface perchlorate salts (Quinn et al., 2013). However these results point to a long-term accumulation of O_2 in the Martian soil; the production rate of O_2 from perchlorate radiolysis is insufficient to produce the observed recurring unexplained signal. More specifically, based on the Quinn et al. (2013) experimental radiation dose and yield, and on their estimated Martian dose rates and estimated 2-m cosmic ray penetration depth, it would take on order of 1 Myr to accumulate enough trapped O_2 for one season worth of 10^{20} molecules cm^{-2} of column O_2 variation. Similarly, the proposed "superoxide" O_2^- ions, suggested to explain the results of the Viking soil reactivity experiments, could form from ultraviolet radiation on surface minerals and lead to the observed release of O_2 with humidification (Yen et al., 2000), but the reported rate of superoxide generation is too small to be consistent with the inferred column O_2 signal yet again by a factor of ~10^6.

The Viking Gas Exchange experiments released up to 770 nanomoles of O_2 from a 1 cm^3 sample over a period of less than 11 days upon "humidification" at ~10° C (Klein, 1978; Oyama & Berdahl, 1977). If the same abundance of rapidly releasable O_2 was present across 2 m of depth (i.e., 200 cm^3), this would yield the 10^{20} molecules cm^{-2} that would explain the atmospheric measurements. This indicates that sufficient rapidly releasable O_2 is present in the Martian soil, although it is not clear that such a rapid release of O_2 could have occurred at Mars ambient temperatures. More importantly, this serves to illustrate that explaining a one-time release of O_2 is not the main problem. The primary difficulty is that the slow rates of accumulation in the processes considered so far cannot explain the seasonal recurrence of excess O_2.

Hydrogen peroxide is worth considering as a solution to this problem, because it is less stable than perchlorates, and is therefore more likely to provide a rapidly exchangeable reservoir of O_2. H_2O_2 has been detected in the atmosphere (Clancy et al., 2004; Encrenaz et al., 2004) and exhibits seasonal and interannual variability (Encrenaz et al., 2019), and it has been suggested that diffusion of atmospheric H_2O_2 into the regolith and/or mineral/water interactions could supply H_2O_2 in the near subsurface (Bullock et al., 1994; Lasne et al., 2016).

Current knowledge of H_2O_2 physics and chemistry in Martian soil is very limited, but based on a coupled soil-atmosphere model by Bullock et al. (1994), it appears that the magnitude and thermal sensitivity of H_2O_2 soil adsorption is potentially close to the right order of magnitude to supply the unexpected 10^{20} molecules cm^{-2} of O_2. However, this conclusion only follows from assuming a 10^7-year chemical lifetime for adsorbed H_2O_2, which is the longest that Bullock et al. (1994) considered plausible, and it depends on their adopted absorption isotherm, which was based on the Fanale and Cannon (1971) empirically derived expression for H_2O since no data for H_2O_2 were available. Furthermore, once the depth penetration of the annual temperature wave (e.g., Grott et al., 2007) is considered, the amount of H_2O_2 potentially cycled in and out of the soil is estimated at an order of magnitude less than needed here, at 10^{19} molecules cm^{-2}. Further, the timescale for diffusion from meter-scale depths may be far too long. Finally, note that although seasonal trends are in fact observed for atmospheric H_2O_2, this mechanism would require a rapid conversion to O_2 immediately at the surface as the observed amount of H_2O_2 is only on the order of ppb (Encrenaz et al., 2015).

Another potential mechanism involving H_2O_2 was proposed by Quinn and Zent (1999). They showed that H_2O_2-TiO_2 complexes rapidly released O_2 upon humidification at warm (for Mars) temperatures of 10 °C; a more extensive study of regolith analogs and environmental conditions for this type of H_2O_2 O_2 conversion in the regolith is needed.

Finally, any release of O_2 to the atmosphere from surface/subsurface reservoirs of H_2O_2 and perchlorates (ClO_4^-) would be associated with concomitant flux of hydrogen and chlorine, respectively, which would impact the chemistry of the atmosphere in ways not seen as well as require their removal from the atmosphere by processes that are poorly understood.

4.2.2. Correlations With CH_4 and Environmental Parameters

The in situ CH_4 abundances measured by SAM/TLS (Webster et al., 2018) are plotted with the relative instantaneous O_2 mixing ratios in Figure 12b. Here, the annual global mean pressure correction is omitted, and the CH_4 data are normalized to the value at L_S 330°, whereas the O_2 data are normalized to L_S 344.9° (Figure 12a). Although not displayed on identical vertical scales, it can be seen that both trace gases exhibit seasonal variations with much greater amplitudes than Ar and N_2 (Figure 12a). The available CH_4 data indicate a smoother seasonal trend than the O_2 within the sampling frequency. The observed behavior of either molecule is not currently understood, and a strong relationship between the two might inform the root cause of observed changes in both O_2 and CH_4, such as the potential seepage or release mechanisms hypothesized for CH_4 (Moores et al., 2019). However, it appears that the O_2 and CH_4 show a similar trend for only part of the year. In particular, the relative decrease during northern fall into winter (as the smaller of the two polar caps forms) is similar for both species. This is a period when O_2 also more closely follows the Ar and N_2 measurements as well as the modeled seasonal trends. Yet in the northern spring/summer, O_2 shows an earlier increase and much more interannual variability than the CH_4 measurements (see Figure 13a for O_2 and CH_4 vs. sol). Thus it seems that at least some component of the variability in the O_2 cycle is unique or not directly affected by the processes that regulate CH_4. Seemingly, with respect to O_2 and CH_4 on Mars, the observations to date are inconclusive as to whether there is a definitive correlation between the them.

Finally, we tested correlations between O_2 abundance variations with a wide range of environmental parameters in an attempt to explain the compositional variability. For most parameters, no correlations were observed (discussed in more detail in Figure S6). Figure 13 shows the correlations identified between $O_2/^{40}Ar$ and the dust opacity and UV absorption in the atmosphere. An overlay of $O_2/^{40}Ar$ ratios and dust opacity as a function of MSL sol number (Figure 13a and Figure S6) suggests some type of inverse relationship between dust opacity and oxygen abundance. A similar relationship is apparent in comparisons with atmospheric UV absorption (Figure 13b and Figure S7). Note that dust opacity and atmospheric UV
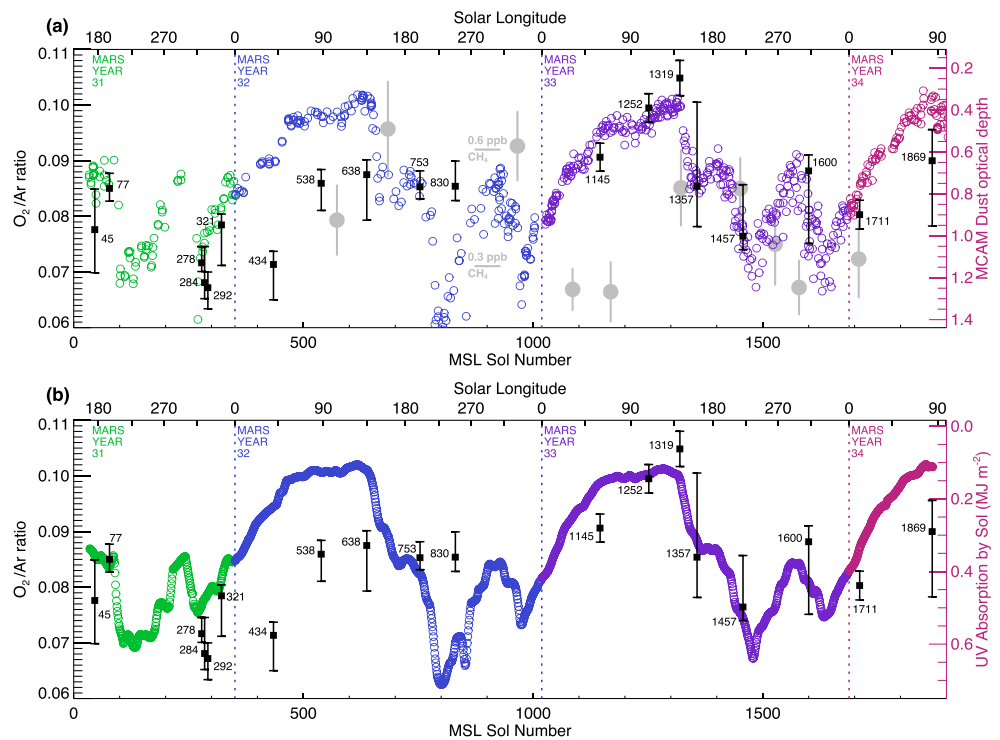
Figure 13. Ratios of $O_2/^{40}Ar$ (black squares with sol numbers) compared with **(a)** dust optical depth (colored circles) and **(b)** UV atmospheric absorption, as a function of MSL mission sol number. Symbol color (and vertical lines) delineate Mars years. The dust opacity axis is reversed, because $O_2/^{40}Ar$ and dust opacity appear to be inversely related. SAM/TLS high-precision enrichment measurements of CH_4 volume mixing ratio are shown as gray circles in the top panel, as described in Webster et al. (2018). CH_4 volume mixing ratio values are shown on a different vertical scale, indicated by horizontal ticks near sol 900. Dust opacity data have been previously described (Martínez et al., 2017; Smith et al., 2016; Vicente-Retortillo et al., 2017; Vicente-Retortillo et al., 2018). Absorption energies are integrated over each sol, and derived from the model of Vicente-Retortillo et al. (2017, 2015).

absorption are closely related, because atmospheric UV absorption is more sensitive to variation in dust loading than to insolation.

The observed correlations are not very strong, with reduced χ_v^2 values significantly greater than 1 (Figures S6c and S7c). This suggests that if a real relationship between atmospheric dust loading (and/or atmospheric UV absorption) is present, that relationship is more complex than a simple linear relationship. Agreement between these dust-related environmental parameters and the O_2 abundance seems weaker in MY 32, compared to the other Mars years. Within the limitations of this analysis, a real relationship between O_2 abundance and atmospheric dust loading (and/or atmospheric UV absorption) could suggest either unknown photochemical or surface chemistry controls on the O_2 abundance.

Thus, the observed O_2 variability remains a mystery until further measurements, models, or experiments are able to identify likely mechanisms through which the O_2 can vary on short timescales. It is hoped that hypotheses that may be testable with further in situ measurements by Curiosity arise, while the mission is still operating in Gale Crater.

5. Summary

The atmospheric compositional data obtained by the SAM instrument in Gale Crater offer unprecedented seasonal and multiyear coverage of the Mars atmosphere at the surface. The abundances of the major atmospheric gases CO_2, N_2, ^{40}Ar, O_2, and CO have been measured from MY 31–MY 34, through three full Martian seasonal cycles. Measurements were sufficiently distributed throughout the mission to provide insight on the behavior of the major atmospheric components in response to the seasonal variations driven by Mars' obliquity and its large orbital eccentricity.

The SAM measurements of volume mixing ratios reveal repeatable cycles in which CO_2 is modulated by the formation and sublimation of the polar caps, but with a lag of approximately 20–40° of L_S behind the maxima and minima of the total pressure cycle. Similarly, the inert tracer species N_2 and Ar show a similar delayed response to the pressure cycle. These data demonstrate that transport acts very rapidly to maintain pressure equilibrium, but changes in VMRs lag behind because physical mixing of air masses is a slower process. Our measurements indicate that for any single location on Mars, the instantaneous composition cannot be simply calculated from the time of year and globally averaged pressure.

Surprisingly, however, we have found that O_2 does not demonstrate the predictable seasonal behavior of the other major components. Surface O_2 measurements by SAM yield abundances that vary between 1300 and 2200 ppmv; when corrected for the annual global mean pressure, O_2 varies from 1300 to 1900 ppmv. Despite large instrument backgrounds, these are the first precise in situ measurements of O_2, revealing a surprising seasonal and interannual variation that cannot be accounted for in current chemical models. Though Mars has the potential to generate significant O_2 release due to abundances of oxidants in/at its surface, the mechanisms by which O_2 could be quickly generated and then quickly destroyed are completely unknown. As with all surprising results, we hope that continued in situ, experimental, and theoretical results may shed light on this intriguing observation.

Observations by MSL and SAM in Gale Crater, such as the atmospheric composition study presented in this paper, have enhanced our understanding of Mars as a complex planetary system. Geophysical and geochemical results have painted a picture of a formerly habitable planet billions of years in Mars' past, and measurements of current processes provide indications that Mars may still potentially harbor habitable environments. The new insights gained on the annual cycle of CO_2, N_2, and Ar presented here enable a more accurate understanding of the seasonal transport and mixing of the bulk atmosphere, thereby improving our ability to track the sources and sinks of trace species such as water and methane. Further, the significant O_2 variability, especially when considered with recently documented seasonal enhancements of CH_4 (Webster et al., 2018), hints at an active present-day Mars.

References

Atreya, S. K., & Gu, Z. G. (1994). Stability of the Martian atmosphere—Is heterogeneous catalysis essential? *Journal of Geophysical Research*, *99*(E6), 13,133–13,145.

Atreya, S. K., & Gu, Z. G. (1995). Photochemistry and stability of the atmosphere of Mars. *Advances in Space Research*, *16*(6), 57–68.

Atreya, S. K., Wong, A. S., Renno, N. O., Farrell, W. M., Delory, G. T., Sentman, D. D., et al. (2006). Oxidant enhancement in Martian dust devils and storms: Implications for life and habitability. *Astrobiology*, *6*(3), 439–450. https://doi.org/10.1089/ast.2006.6.439

Barker, E. S. (1972). Detection of molecular oxygen in Martian atmosphere. *Nature*, *238*(5365), 447–448. https://doi.org/10.1038/238447a0

Becker, R. H., & Pepin, R. O. (1984). The case for a martian origin of the shergottites— nitrogen and the noble gases in EETA-79001. *Earth and Planetary Science Letters*, *69*(2), 225–242. https://doi.org/10.1016/0012-821x(84)90183-3

Billebaud, F., Brillet, J., Lellouch, E., Fouchet, T., Encrenaz, T., Cottini, V., et al. (2009). Observations of CO in the atmosphere of Mars with PFS onboard Mars Express. *Planetary and Space Science*, *57*(12), 1446–1457. https://doi.org/10.1016/j.pss.2009.07.004

Bullock, M. A., Stoker, C. R., McKay, C. P., & Zent, A. P. (1994). A coupled soil atmosphere model of H_2O_2 on Mars. *Icarus*, *107*(1), 142–154. https://doi.org/10.1006/icar.1994.1012

Carleton, N. P., & Traub, W. A. (1972). Detection of molecular oxygen on Mars. *Science*, *177*(4053), 988–992. https://doi.org/10.1126/science.177.4053.988

Clancy, R. T., Sandor, B. J., & Moriarty-Schieven, G. H. (2004). A measurement of the 362 GHz absorption line of Mars atmospheric H_2O_2. *Icarus*, *168*(1), 116–121. https://doi.org/10.1016/j.icarus.2003.12.003

Encrenaz, T., Fouchet, T., Melchiorri, R., Drossart, P., Gondet, B., Langevin, Y., et al. (2006). Seasonal variations of the Martian CO over Hellas as observed by OMEGA/Mars express. *Astronomy & Astrophysics*, *459*(1), 265–270. https://doi.org/10.1051/0004-6361:20065586

Encrenaz, T., Greathouse, T. K., Aoki, S., Daerden, F., Giuranna, M., Forget, F., et al. (2019). Ground-based infrared mapping of H_2O_2 on Mars near opposition. *Astronomy & Astrophysics*, *627*, A60. https://doi.org/10.1051/0004-6361/201935300

Encrenaz, T., Greathouse, T. K., Lefèvre, F., Montmessin, F., Forget, F., Fouchet, T., et al. (2015). Seasonal variations of hydrogen peroxide and water vapor on Mars: Further indications of heterogeneous chemistry. *Astronomy & Astrophysics*, *578*, A127. https://doi.org/10.1051/0004-6361/201425448

Encrenaz, T., Lellouch, E., Atreya, S. K., & Wong, A. S. (2004). Detectability of minor constituents in the Martian atmosphere by infrared and submillimeter spectroscopy. *Planetary and Space Science*, *52*(11), 1023–1037.

England, C., & Hrubes, J. D. (2004). Molecular oxygen mixing ratio and its seasonal variability in the Martian atmosphere, paper presented at Workshop on Oxygen in the Terrestrial Planets.

Fanale, F. P., & Cannon, W. A. (1971). Adsorption on Martian regolith. *Nature*, *230*(5295), 502–504. https://doi.org/10.1038/230502a0

Formisano, V., Atreya, S., Encrenaz, T., Ignatiev, N., & Giuranna, M. (2004). Detection of methane in the atmosphere of Mars. *Science*, *306*(5702), 1758–1761. https://doi.org/10.1126/science.1101732

Franz, H. B., Trainer, M. G., Malespin, C. A., Mahaffy, P. R., Atreya, S. K., Becker, R. H., et al. (2017). Initial SAM calibration gas experiments on Mars: Quadrupole mass spectrometer results and implications. *Planetary and Space Science*, *138*, 44–54. https://doi.org/10.1016/j.pss.2017.01.014

Franz, H. B., Trainer, M. G., Wong, M. H., Mahaffy, P. R., Atreya, S. K., Manning, H. L. K., & Stern, J. C. (2015). Reevaluated Martian atmospheric mixing ratios from the mass spectrometer on the Curiosity rover. *Planetary and Space Science*, *109-110*, 154–158. https://doi.org/10.1016/j.pss.2015.02.014

Franz, H. B., Trainer, M. G., Wong, M. H., Manning, H. L. K., Stern, J. C., Mahaffy, P. R., et al. (2014). Analytical techniques for retrieval of atmospheric gas abundances and isotope ratios measured by the quadrupole mass spectrometer of the sample analysis at mars instrument suite on Mars Science Laboratory. *Planetary and Space Science*, *96*, 99–113. https://doi.org/10.1016/j.pss.2014.03.005

Frigstad, H., Andersen, T., Hessen, D. O., Naustvoll, L. J., Johnsen, T. M., & Bellerby, R. G. J. (2011). Seasonal variation in marine CNP stoichiometry: Can the composition of seston explain stable Redfield ratios? *Biogeosciences*, *8*(10), 2917–2933. https://doi.org/10.5194/bg-8-2917-2011

Gómez-Elvira, J., Armiens, C., Castañer, L., Domínguez, M., Genzer, M., Gómez, F., et al. (2012). REMS: The environmental sensor suite for the Mars Science Laboratory rover. *Space Science Reviews*, *170*(1-4), 583–640. https://doi.org/10.1007/s11214-012-9921-1

Grott, M., Helbert, J., & Nadalini, R. (2007). Thermal structure of Martian soil and the measurability of the planetary heat flow. *Journal of Geophysical Research*, *112*, E09004. https://doi.org/10.1029/2007JE002905

Haberle, R. M., Gómez-Elvira, J., de la Torre Juárez, M., Harri, A. M., Hollingsworth, J. L., Kahanpää, H., et al., & REMS/MSL Science Teams (2014). Preliminary interpretation of the REMS pressure data from the first 100 sols of the MSL mission. *Journal of Geophysical Research: Planets*, *119*, 440–453. https://doi.org/10.1002/2013JE004488

Harri, A. M., Genzer, M., Kemppinen, O., Kahanpää, H., Gomez-Elvira, J., Rodriguez-Manfredi, J. A., et al. (2014). Pressure observations by the Curiosity rover: Initial results. *Journal of Geophysical Research: Planets*, *119*, 82–92. https://doi.org/10.1002/2013JE004423

Hartogh, P., Błęcka, M. I., Jarchow, C., Sagawa, H., Lellouch, E., de Val-Borro, M., et al. (2010). First results on Martian carbon monoxide from Herschel/HIFI observations. *Astronomy & Astrophysics*, *521*, L48. https://doi.org/10.1051/0004-6361/201015159

Hartogh, P., Jarchow, C., Lellouch, E., de Val-Borro, M., Rengel, M., Moreno, R., et al. (2010). Herschel/HIFI observations of Mars: First detection of O_2 at submillimetre wavelengths and upper limits on HCl and H_2O_2. *Astronomy & Astrophysics*, *521*, L49. https://doi.org/10.1051/0004-6361/201015160

Hecht, M. H., Kounaves, S. P., Quinn, R. C., West, S. J., Young, S. M., Ming, D. W., et al. (2009). Detection of perchlorate and the soluble chemistry of Martian soil at the Phoenix Lander site. *Science*, *325*(5936), 64–67. https://doi.org/10.1126/science.1172466

Hess, S. L., Ryan, J. A., Tillman, J. E., Henry, R. M., & Leovy, C. B. (1980). The annual cycle of pressure on Mars measured by Viking Lander 1 and Viking Lander 2. *Geophysical Research Letters*, *7*(3), 197–200. https://doi.org/10.1029/GL007i003p00197

James, P. B., Kieffer, H. H., & Paige, D. A. (1992). The seasonal cycle of carbon dioxide on Mars. In H. H. Kieffer (Ed.), *Mars*, (pp. 934–968). Tuscon, Ariz: Univ. of Ariz. Press.

Johnson, J. R., Bell, J. F. III, Bender, S., Blaney, D., Cloutis, E., DeFlores, L., et al. (2015). ChemCam passive reflectance spectroscopy of surface materials at the Curiosity landing site, Mars. *Icarus*, *249*, 74–92. https://doi.org/10.1016/j.icarus.2014.02.028

Klein, H. P. (1978). Viking biological experiments on Mars. *Icarus*, *34*(3), 666–674. https://doi.org/10.1016/0019-1035(78)90053-2

Klingler, J. M., Mancinelli, R. L., & White, M. R. (1989). Biological nitrogen fixation under primordial Martian partial pressures of dinitrogen. *Advances in Space Research*, *9*(6), 173–176. https://doi.org/10.1016/0273-1177(89)90225-1

Krasnopolsky, V. A. (1993). Photochemistry of the Martian atmosphere (Mean Conditions). *Icarus*, *101*(2), 313–332. https://doi.org/10.1006/icar.1993.1027

Krasnopolsky, V. A. (2003). Spectroscopic mapping of Mars CO mixing ratio: Detection of north-south asymmetry. *Journal of Geophysical Research*, *108*(E2), 5010. https://doi.org/10.1029/2002JE001926

Krasnopolsky, V. A. (2010). Solar activity variations of thermospheric temperatures on Mars and a problem of CO in the lower atmosphere. *Icarus*, *207*(2), 638–647. https://doi.org/10.1016/j.icarus.2009.12.036

Krasnopolsky, V. A. (2015). Variations of carbon monoxide in the Martian lower atmosphere. *Icarus*, *253*, 149–155. https://doi.org/10.1016/j.icarus.2015.03.006

Krasnopolsky, V. A. (2017). Annual mean mixing ratios of N_2, Ar, O_2, and CO in the Martian atmosphere. *Planetary and Space Science*, *144*, 71–73. https://doi.org/10.1016/j.pss.2017.05.009

Krasnopolsky, V. A., Maillard, J. P., & Owen, T. C. (2004). Detection of methane in the Martian atmosphere: Evidence for life? *Icarus*, *172*(2), 537–547.

Lasne, J., Noblet, A., Szopa, C., Navarro-Gonzalez, R., Cabane, M., Poch, O., et al. (2016). Oxidants at the surface of Mars: A review in light of recent exploration results. *Astrobiology*, *16*(12), 977–996. https://doi.org/10.1089/ast.2016.1502

Lefèvre, F., & Krasnopolsky, V. A. (2017). Atmospheric photochemistry. In R. Haberle, R. T. Clancy, F. Forget, M. Smith, & R. W. Zurek (Eds.), *The Atmosphere and Climate of Mars* (pp. 405–432). Cabridge: Cambridge University Press. https://doi.org/10.1017/9781139060172.013

Lefevre, F., Lebonnois, S., Montmessin, F., & Forget, F. (2004). Three-dimensional modeling of ozone on Mars. *Journal of Geophysical Research*, *109*, E07004. https://doi.org/10.1029/2004JE002268

Leigh, J. A. (2000). Nitrogen fixation in methanogens: The archaeal perspective. *Current Issues in Molecular Biology*, *2*, 125–131.

Lian, Y., Richardson, M. I., Newman, C. E., Lee, C., Toigo, A. D., Mischna, M. A., & Campin, J. M. (2012). The Ashima/MIT Mars GCM and argon in the martian atmosphere. *Icarus*, *218*(2), 1043–1070. https://doi.org/10.1016/j.icarus.2012.02.012

Mahaffy, P. R., Webster, C. R., Atreya, S. K., Franz, H., Wong, M., Conrad, P. G., et al., & MSL Science Team (2013). Abundance and isotopic composition of gases in the Martian atmosphere from the Curiosity rover. *Science*, *341*(6143), 263–266. https://doi.org/10.1126/science.1237966

Mahaffy, P. R., Webster, C. R., Cabane, M., Conrad, P. G., Coll, P., Atreya, S. K., et al. (2012). The sample analysis at Mars investigation and instrument suite. *Space Science Reviews*, *170*(1-4), 401–478. https://doi.org/10.1007/s11214-012-9879-z

Malespin, C. A., Freissinet, C., Glavin, D., Mahaffy, P., Millan, M., Buch, A., et al. (2018). The first complete SAM wet chemistry experiment on Mars, paper presented at the *49th Lunar and Planetary Science Conference*, LPI Contribution No. 2083, The Woodlands, TX.

Martínez, G. M., Fischer, E., Rennó, N. O., Sebastián, E., Kemppinen, O., Bridges, N., et al. (2016). Likely frost events at Gale Crater: Analysis from MSL/REMS measurements. *Icarus*, *280*, 93–102. https://doi.org/10.1016/j.icarus.2015.12.004

Martínez, G. M., Newman, C. N., Vicente-Retortillo, A., Fischer, E., Renno, N. O., Richardson, M. I., et al. (2017). The modern near-surface Martian climate: A review of in situ meteorological data from Viking to Curiosity. *Space Science Reviews*, *212*(1-2), 295–338. https://doi.org/10.1007/s11214-017-0360-x

Maurice, S., Wiens, R. C., Saccoccio, M., Barraclough, B., Gasnault, O., Forni, O., et al. (2012). The ChemCam instrument suite on the Mars Science Laboratory (MSL) rover: Science objectives and mast unit description. *Space Science Reviews*, *170*(1-4), 95–166. https://doi.org/10.1007/s11214-012-9912-2

McConnochie, T. H., Smith, M. D., Wolff, M. J., Bender, S., Lemmon, M., Wiens, R. C., et al. (2017a). Retrieval of water vapor column abundance and aerosol properties from ChemCam passive sky spectroscopy. *Icarus*, *307*, 294–326. https://doi.org/10.1016/j. icarus.2017.10.043

McConnochie, T. H., Smith, M. D., Wolff, M. J., Bender, S., Lemmon, M., Wiens, R. C., et al. (2018). Retrieval of water vapor column abundance and aerosol properties from ChemCam passive sky spectroscopy. *Icarus*, *307*, 294–326. https://doi.org/10.1016/j. icarus.2017.10.043

McConnochie, T. H., Smith, M. D., Wolff, M. J., Bender, S. C., Lemmon, M. T., Wiens, R. C., et al. (2017b). ChemCam passive sky spectroscopy at Gale Crater: Interannual variability in dust aerosol particle size, missing water vapor, and the molecular oxygen problem, *Paper presented at American Geophysical Union Fall Meeting*, New Orleans, LA.

Menge, D. N. L., Reed, S. C., & Cleveland, C. C. (2013). Biological nitrogen fixation: rates, patterns and ecological controls in terrestrial ecosystems. *Philosophical Transactions of the Royal Society London B*, *368*(1621), 20130119. https://doi.org/10.1098/rstb.2013.0119

Montmessin, F., Korablev, O., Lefèvre, F., Bertaux, J. L., Fedorova, A., Trokhimovskiy, A., et al. (2017). SPICAM on Mars Express: A 10-year in-depth survey of the Martian atmosphere. *Icarus*, *297*, 195–216. https://doi.org/10.1016/j.icarus.2017.06.022

Moores, J. E., Gough, R. V., Martinez, G. M., Meslin, P. Y., Smith, C. L., Atreya, S. K., et al. (2019). Methane seasonal cycle at Gale Crater on Mars consistent with regolith adsorption and diffusion. *Nature Geoscience*, *12*(5), 321–325. https://doi.org/10.1038/s41561-019-0313-y

Mumma, M. J., Villanueva, G. L., Novak, R. E., Hewagama, T., Bonev, B. P., DiSanti, M. A., et al. (2009). Strong release of methane on Mars in northern summer 2003. *Science*, *323*(5917), 1041–1045. https://doi.org/10.1126/science.1165243

Navarro-Gonzalez, R., McKay, C. P., & Mvondo, D. N. (2001). A possible nitrogen crisis for Archaean life due to reduced nitrogen fixation by lightning. *Nature*, *412*(6842), 61–64. https://doi.org/10.1038/35083537

Navarro-Gonzalez, R., Molina, M. J., & Molina, L. T. (1998). Nitrogen fixation by volcanic lightning in the early Earth. *Geophysical Research Letters*, *25*(16), 3123–3126. https://doi.org/10.1029/98GL02423

Navarro-Gonzalez, R., Navarro, K. F., Coll, P., McKay, C. P., Stern, J. C., Sutter, B., et al. (2019). Abiotic input of fixed nitrogen by bolide impacts to Gale Crater during the Hesperian: Insights from the Mars Science Laboratory. *Journal of Geophysical Research: Planets*, *124*, 94–113. https://doi.org/10.1029/2018JE005852

Newman, C. E., Gómez-Elvira, J., Marin, M., Navarro, S., Torres, J., Richardson, M. I., et al. (2017). Winds measured by the Rover Environmental Monitoring Station (REMS) during the Mars Science Laboratory (MSL) rover's Bagnold Dunes campaign and comparison with numerical modeling using MarsWRF. *Icarus*, *291*, 203–231. https://doi.org/10.1016/j.icarus.2016.12.016

Nier, A. O., & McElroy, M. B. (1977). Composition and structure of Mars' upper atmosphere: Results from the neutral mass spectrometers on Viking 1 and 2. *Journal of Geophysical Research*, *82*(28), 4341–4349. https://doi.org/10.1029/JS082i028p04341

Owen, T. (1992). The composition and early history of the atmosphere of Mars. In H. Kieffer, B. M. Jakosky, C. Snyder, & M. S. Matthews (Eds.), *Mars* (pp. 818–835). Tucson, AZ: University of Arizona Press.

Owen, T., & Biemann, K. (1976). Composition of the atmosphere at the surface of Mars: Detection of argon-36 and preliminary analysis. *Science*, *193*(4255), 801–803. https://doi.org/10.1126/science.193.4255.801

Owen, T., Biemann, K., Rushneck, D. R., Biller, J. E., Howarth, D. W., & Lafleur, A. L. (1977). The composition of the atmosphere at the surface of Mars. *Journal of Geophysical Research*, *82*(28), 4635–4639. https://doi.org/10.1029/JS082i028p04635

Oyama, V. I., & Berdahl, B. J. (1977). The Viking Gas Exchange experiment results from Chryse and Utopia surface samples. *Journal of Geophysical Research*, *82*(28), 4669–4676. https://doi.org/10.1029/JS082i028p04669

Pla-Garcia, J., Rafkin, S. C. R., Kahre, M., Gomez-Elvira, J., Hamilton, V. E., Navarro, S., et al. (2016). The meteorology of Gale crater as determined from rover environmental monitoring station observations and numerical modeling. Part I: Comparison of model simulations with observations. *Icarus*, *280*, 103–113. https://doi.org/10.1016/j.icarus.2016.03.013

Quinn, R. C., Martucci, H. F. H., Miller, S. R., Bryson, C. E., Grunthaner, F. J., & Grunthaner, P. J. (2013). Perchlorate radiolysis on Mars and the origin of Martian soil reactivity. *Astrobiology*, *13*(6), 515–520. https://doi.org/10.1089/ast.2013.0999

Quinn, R. C., & Zent, A. P. (1999). Peroxide-modified titanium dioxide: A chemical analog of putative Martian soil oxidants. *Origins of Life and Evolution of Biospheres*, *29*(1), 59–72.

Rafkin, S., J. Pla-Garcia, C. Newman, V. Hamilton, J. Martin-Torres, M. P. Zorzano, et al. (2014), The meteorology of Gale Crater determined from REMS data and mesoscale modeling, paper presented at Eighth International Conference on Mars, LPI Contribution No. 1158, Pasadena, CA.

Rafkin, S. C. R., Pla-Garcia, J., Kahre, M., Gomez-Elvira, J., Hamilton, V. E., Marín, M., et al. (2016). The meteorology of Gale Crater as determined from Rover Environmental Monitoring Station observations and numerical modeling. Part II: Interpretation. *Icarus*, *280*, 114–138. https://doi.org/10.1016/j.icarus.2016.01.031

Sandel, B. R., Groller, H., Yelle, R. V., Koskinen, T., Lewis, N. K., Bertaux, J. L., et al. (2015). Altitude profiles of O_2 on Mars from SPICAM stellar occultations. *Icarus*, *252*, 154–160. https://doi.org/10.1016/j.icarus.2015.01.004

Schumann, U., & Huntrieser, H. (2007). The global lightning-induced nitrogen oxides source. *Atmospheric Chemistry and Physics*, *7*(14), 3823–3907. https://doi.org/10.5194/acp-7-3823-2007

Segura, A., & Navarro-Gonzalez, R. (2005). Nitrogen fixation on early Mars by volcanic lightning and other sources. *Geophysical Research Letters*, *32*, L05203. https://doi.org/10.1029/2004GL021910

Sindoni, G., Formisano, V., & Geminale, A. (2011). Observations of water vapor and carbon monoxide in the Martian atmosphere with the SWC of PFS/MEX. *Planetary and Space Science*, *59*(2–3), 149–162. https://doi.org/10.1016/j.pss.2010.12.006

Smith, M. D., Daerden, F., Neary, L., & Khayat, A. (2017). The climatology of carbon monoxide and water vapor on Mars as observed by CRISM and modeled by the GEM-Mars general circulation model. *Icarus*. https://doi.org/10.1016/j.icarus.2017.09.027

Smith, M. D., Wolff, M. J., Clancy, R. T., & Murchie, S. L. (2009). Compact reconnaissance imaging spectrometer observations of water vapor and carbon monoxide. *Journal of Geophysical Research*, *114*, E00D03. https://doi.org/10.1029/2008JE003288

Smith, M. D., Zorzano, M. P., Lemmon, M., Martin-Torres, J., & de Cal, T. M. (2016). Aerosol optical depth as observed by the Mars Science Laboratory REMS UV photodiodes. *Icarus*, *280*, 234–248. https://doi.org/10.1016/j.icarus.2016.07.012

Sprague, A. L., Boynton, W. V., Forget, F., Lian, Y., Richardson, M., Starr, R., et al. (2012). Interannual similarity and variation in seasonal circulation of Mars' atmospheric Ar as seen by the gamma ray spectrometer on Mars Odyssey. *Journal of Geophysical Research*, *117*, E04005. https://doi.org/10.1029/2011JE003873

Sprague, A. L., Boynton, W. V., Kerry, K. E., Janes, D. M., Kelly, N. J., Crombie, M. K., et al. (2007). Mars' atmospheric argon: Tracer for understanding Martian atmospheric circulation and dynamics. *Journal of Geophysical Research*, *112*, E03S02. https://doi.org/10.1029/2005JE002597

Stern, J. C., Sutter, B., Freissinet, C., Navarro-González, R., McKay, C., Archer PD Jr, et al., & MSL Science Team (2015). Evidence for indigenous nitrogen in sedimentary and aeolian deposits from the Curiosity rover investigations at Gale Crater, Mars. *PNAS*, *112*(14), 4245–4250. https://doi.org/10.1073/pnas.1420932112

Stern, J. C., Sutter, B., Jackson, W. A., Navarro-Gonzalez, R., McKay, C. P., Ming, D. W., et al. (2017). The nitrate/(per)chlorate relationship on Mars. *Geophysical Research Letters*, *44*, 2643–2651. https://doi.org/10.1002/2016GL072199

Sutter, B., McAdam, A. C., Mahaffy, P. R., Ming, D. W., Edgett, K. S., Rampe, E. B., et al. (2017). Evolved gas analyses of sedimentary rocks and eolian sediment in Gale Crater, Mars: Results of the Curiosity rover's sample analysis at Mars instrument from Yellowknife Bay to the Namib Dune. *Journal of Geophysical Research: Planets*, *122*, 2574–2609. https://doi.org/10.1002/2016JE005225

Tillman, J. E., Johnson, N. C., Guttorp, P., & Percival, D. B. (1993). The Martian annual atmospheric pressure cycle: Years without great dust storms. *Journal of Geophysical Research*, *84*, 10,963–910,971.

Trainer, M. G. (2019a). Daily mean pressure and temperature for the surface of Mars from MSL/REMS, https://doi.org/10.7910/DVN/OYSRDP

Trainer, M. G. (2019b). Volume mixing ratios of major atmospheric components on Mars as measured by MSL/SAM, https://doi.org/10.7910/DVN/CVUOWW

Trauger, J. T., & Lunine, J. I. (1983). Spectroscopy of molecular oxygen in the atmospheres of Venus and Mars. *Icarus*, *55*(2), 272–281. https://doi.org/10.1016/0019-1035(83)90082-9

Tyler, D., & Barnes, J. R. (2013). Mesoscale modeling of the circulation in the Gale Crater region: An investigation into the complex forcing of convective boundary layer depths. *Mars*, *8*, 58–77. https://doi.org/10.1555/mars.2013.0003

VanBommel, S. J., Gellert, R., Clark, B. C., & Ming, D. W. (2018). Seasonal atmospheric argon variability measured in the equatorial region of Mars by the Mars exploration rover alpha particle X-ray spectrometers: Evidence for an annual argon-enriched front. *Journal of Geophysical Research: Planets*, *123*, 544–558. https://doi.org/10.1002/2017JE005454

Vasavada, A. R., Grotzinger, J. P., Arvidson, R. E., Calef, F. J., Crisp, J. A., Gupta, S., et al. (2014). Overview of the Mars Science Laboratory mission: Bradbury landing to Yellowknife Bay and beyond. *Journal of Geophysical Research: Planets*, *119*, 1134–1161. https://doi.org/10.1002/2014JE004622

Vicente-Retortillo, A., Martinez, G. M., Renno, N., Newman, C. E., Ordonez-Etxeberria, I., Lemmon, M. T., et al. (2018). Seasonal deposition and lifting of dust on Mars as observed by the Curiosity rover. *Scientific Reports*, *8*(1), 1–8. https://doi.org/10.1038/s41598-018-35946-8

Vicente-Retortillo, Á., Martínez, G. M., Renno, N. O., Lemmon, M. T., & de la Torre-Juárez, M. (2017). Determination ofdust aerosol particle size at Gale Crater using REMS UVS and Mastcam measurements. *Geophysical Research Letters*, *44*, 3502–3508. https://doi.org/10.1002/2017GL072589

Vicente-Retortillo, A., Valero, F., Vazquez, L., & Martinez, G. M. (2015). A model to calculate solar radiation fluxes on the Martian surface. *Journal of Space Weather and Space Climate*, *5*, 13. https://doi.org/10.1051/swsc/2015035

Webster, C. R., Mahaffy, P. R., Atreya, S. K., Flesch, G. J., Farley, K. A., & T. M. S. Team (2013). Low upper limit to methane abundance on Mars. *Science*. https://doi.org/10.1126/science.1242902

Webster, C. R., Mahaffy, P. R., Atreya, S. K., Flesch, G. J., Mischna, M. A., Meslin, P. Y., et al. (2015). Mars methane detection and variability at Gale Crater. *Science*, *347*(6220), 415–417. https://doi.org/10.1126/science.1261713

Webster, C. R., Mahaffy, P. R., Atreya, S. K., Moores, J. E., Flesch, G. J., Malespin, C., et al. (2018). Background levels of methane in Mars' atmosphere show strong seasonal variations. *Science*, *360*(6393), 1093–1096. https://doi.org/10.1126/science.aaq0131

Wiens, R. C., Maurice, S., Barraclough, B., Saccoccio, M., Barkley, W. C., Bell, J. F., et al. (2012). The ChemCam instrument suite on the Mars Science Laboratory (MSL) rover: Body unit and combined system tests. *Space Science Reviews*, *170*(1-4), 167–227. https://doi.org/10.1007/s11214-012-9902-4

Wong, A. S., Atreya, S. K., & Encrenaz, T. (2003). Chemical markers of possible hot spots on Mars. *Journal of Geophysical Research*, *108*(E4), 5026. https://doi.org/10.1029/2002JE002003

Wong, M. H., Atreya, S. K., Mahaffy, P. N., Franz, H. B., Malespin, C., Trainer, M. G., et al. (2013). Isotopes of nitrogen on Mars: Atmospheric measurements by Curiosity's mass spectrometer. *Geophysical Research Letters*, *40*, 6033–6037. https://doi.org/10.1002/2013GL057840

Wong, M. H., LeFavor, M., Newman, C., Prats, B., Kahanpää, H., Genzer, M., et al. (2013). MSL/REMS Measurements of conditions during MSL/SAM atmospheric ingestion events, paper presented at 44th Lunar and Planetary Science Conference, LPI Contribution No. 1719, The Woodlands, TX.

Yen, A. S., Kim, S. S., Hecht, M. H., Frant, M. S., & Murray, B. (2000). Evidence that the reactivity of the Martian soil is due to superoxide ions. *Science*, *289*(5486), 1909–1912. https://doi.org/10.1126/science.289.5486.1909

Yung, Y. L., Strobel, D. F., Kong, T. Y., & McElroy, M. B. (1977). Photochemistry of nitrogen in the Martian atmosphere. *Icarus*, *30*, 26–41. https://doi.org/10.1016/0019-1035(77)90118-X

Zahnle, K., Haberle, R. M., Catling, D. C., & Kasting, J. F. (2008). Photochemical instability of the ancient Martian atmosphere. *Journal of Geophysical Research*, *113*, E11004. https://doi.org/10.1029/2008JE003160

Zehr, J. P., Waterbury, J. B., Turner, P. J., Montoya, J. P., Omoregie, E., Steward, G. F., et al. (2001). Unicellular cyanobacteria fix N_2 in the subtropical North Pacific Ocean. *Nature*, *412*(6847), 635–638. https://doi.org/10.1038/35088063